Precambrian Research 227 (2013) 389–408

Contents lists available at SciVerse ScienceDirect

Precambrian Research

journal homepage: www.elsevier.com/locate/precamres

Petrology of the Neoproterozoic granulites from Central Dronning Maud Land, East Antarctica – Implications for southward extension of East African Orogen (EAO)

N.C. Pant[a,*], A. Kundu[b], M.J. D'Souza[b], Ashima Saikia[a]

[a] Department of Geology, University of Delhi, Delhi 110 007, India
[b] Geological Survey of India, NH-5P, N.I.T., Faridabad 121 001, India

ARTICLE INFO

Article history:
Received 4 December 2011
Received in revised form 7 June 2012
Accepted 25 June 2012
Available online 17 July 2012

Keywords:
East Antarctica
East African Orogen
Granulites
Neoproterozoic
Gondwanaland

ABSTRACT

Suturing of east and west Gondwana occurred during the Neoproterozoic along the East African Orogen (EAO) through continent–continent collision. The southern extension of EAO is projected in central Dronning Maud Land (CDML) in east Antarctica. CDML is considered to be a magmato-metamorphic terrain where high-grade metamorphism occurred during Mesoproterozoic. Granulite grade metamorphic assemblages from metapelites (garnet + sillimanite + K feldspar (perthite) + graphite ± plagioclase + quartz ± melt), mafic granulite (orthopyroxene + garnet ± clinopyroxene + plagioclase + quartz) and granitic orthogneiss (garnet + Fe-clinopyroxene + K feldspar + plagioclase + quartz) in the Humboldt Mountains in CDML have been used to deduce the peak metamorphic conditions as ~850 °C and 6–8 kbar pressure. In situ chemical dating of monazite in matrix and inclusions in garnet indicates metamorphism to have occurred between 640 and 580 Ma and was partially overprinted at ~540 Ma which is correlatable with extensive charnockite and A-type granite emplacements. This Neoproterozoic metamorphism and its correlation with the coast margin Neoproterozoic granulites at Schirmacher oasis is inferred as the extension of EAO in east Antarctica.

© 2012 Elsevier B.V. All rights reserved.

1. Introduction

The idea of existence of a single supercontinent during entire Proterozoic (Piper, 1976) was shown to be inconsistent with the geological and palaeomagnetic evidence. This data can be better explained by assumption of the presence of two separate continental masses, i.e. east and west Gondwana, which came together in Neoproterozoic (McWilliams, 1981; Meert et al., 1995). In the east Gondwana continental block (India, Australia, Antarctica) a continuous Circum-East Antarctic belt of Mesoproterozoic age was considered to be present which implied the presence of a global scale ~Grenville age collisional Orogen all along east Antarctica (Hoffman, 1991). However, the discontinuity of this Mesoproterozoic belt in two major domains, i.e. Dronning Maud Land and Prydz bay-Denman Region Glacier has been well demonstrated in east Antarctica (Fitzsimons, 2000a) by the disrupting presence of Neoproterozoic to Pan-African tectonic belts. Based on analysis of geochronologic data showing disparate histories of tectonometamorphic evolution from three segments of east Antarctica separated by these two Neoproterozoic belts (Fitzsimons, 2000b; Fig. 2), it has been shown that the present day alignment of Mesoproterozoic Circum-East Antarctic belt is a consequence of collision of the east and the west Gondwana blocks. This collision led to suturing of these two continental masses along the Mozambique Belt or the East African Orogen (Stern, 1994) resulting into the Palaeozoic Gondwanaland assembly.

The East African Orogen (EAO) modelled as a continent–continent collision zone (e.g. Collins et al., 2012) has been proposed to extend into east Antarctica (Jacobs et al., 1999) in CDML though its precise extension is not well defined. The issues involved in this reconstruction can be listed as;

1. Lithological continuity of rocks of EAO in the projected area of east Antarctica.
2. Identification and characterization of the suture zone and its extension.
3. Identification of Neoproterozoic metamorphic event consistent with the suturing of east and west Gondwana Land.
4. The geodynamic context of anorogenic magmatism (anorthosite, charnockite, granite) spatially associated with this suture.

In recent years, there have been several studies (e.g. Jacobs et al., 2003; Paulsson and Austrheim, 2003; Mikhalasky et al., 2006) which have attempted to bridge this gap. Granulites representing the 600–660 Ma East African Orogeny (Stern, 1994) have been correlated with those present in a small (~35 km^2) coast-margin

* Corresponding author. Tel.: +91 9953781350; fax: +91 1127666295.
E-mail address: pantnc@rediffmail.com (N.C. Pant).

0301-9268/$ – see front matter © 2012 Elsevier B.V. All rights reserved.
http://dx.doi.org/10.1016/j.precamres.2012.06.013

exposure at Schirmacher Oasis (Ravikant et al., 2004, 2007; Baba et al., 2006) and these have been shown to be late Neoproterozoic. Though there are differences in interpretation of metamorphic paths in Schirmacher oasis from isobaric heating-isothermal decompression-isobaric cooling (Ravikant and Kundu, 1988) to isobaric cooling during retrograde metamorphism (Baba et al., 2006), two major conclusions are apparent in having clockwise P–T–t paths and the timing of peak metamorphism to be significantly younger than envisaged earlier (Baba et al., 2008, 2010), thus establishing an affinity with the EAO. However, characterization of definite Neoproterozoic metamorphism, evaluating the metamorphic conditions and establishing its context in terms of East African Orogen (EAO) has not been done from the Wohlthat Massif which represents the main outcrop area of the CDML. The present work attempts to fill this gap by evaluating metamorphic conditions and providing age constraints from metapelites and orthogneisses.

2. Geological setting

The Central Dronning Maud Land (CDML) in east Antarctica (Boger, 2011) is characterized by two major types of rock exposures. The northernmost of these is the Schirmacher oasis representing a smaller (~35 km^2), coast-marginal area and ~80 km south, a much larger group of exposures (several hundred km^2) known as Wohlthat massif with Gruber mountains in the east, the Petermann ranges in the centre and the Humboldt mountains towards west (Fig. 1). The Sør Rondane Mountains towards east and the Mühlig Hofman Mountains towards west are the major rock outcrops on the two sides of the Wohlthat massif. In eastern parts of CDML (Gruber Mountains and Petrmann ranges) large exposures of plutonic rocks occur (Gruber anorthosites, Ravich and Soloviev, 1966; A-type granite, Joshi et al., 1991) describing the anorthosite–mangerite–charnockite–granite (AMCG) association (Joshi and Pant, 1995; Mikhalasky et al., 2006) while the western part of the CDML (Humboldt Mountains) is dominantly composed of metamorphics (Fig. 1) with sedimentary precursors in the northern part and the orthogneisses in the southern part (Humboldt Series of Ravich and Kamenev, 1975). Based on petrologic and tectonic comparison with other protogeosynclinal sequences in Gondwanaland, Ravich and Kamenev (1975) assigned upper Archaean ages to the Humboldt Series while gneisses in the Humboldt Mountains were considered middle Proterozoic in some subsequent correlations (James and Tingey, 1983; Yoshida and Kizaki, 1983). Additional geochronological data (Jacobs et al., 1998, 1999) indicated 1080 ± 10 Ma as the age of first major metamorphic event in CDML. This was based on age derived from zircons from the volcanic and sheet like intrusives in the Humboldt Mountains and adjacent areas. The widespread magmatic activity has three major components in CDML viz. anorthosite, charnockites and granites. Anorthosites have been dated at ~600 Ma (Jacobs et al., 1998), charnockites at ~510 Ma (Mikhalasky et al., 1997) and the granite at ~500 Ma (Bisnath et al., 2006) all indicating post peak-metamorphism extensional components possibly in two phases. This succeeded a compressional phase of penetrative foliation development and high grade peak metamorphism. Generally the development of penetrative foliation has been ascribed Mesoproterozoic age (Groenewald et al., 1995; Grantham et al., 1995).

The metasedimentary-orthogneiss metamorphites in the Humboldt Mountains preserve evidence of polyphase deformation. The first phase of deformation (D1) is present as rarely preserved, small scale interfolial folds (F1). These folds are nearly coaxial with the folds produced by second episode of deformation (D2). These F2 folds are tight isoclinals to nearly recumbent. Regional strike of the foliation of these rocks is nearly east–west with the average dip of ~25°. A metamorphic sequence of >8 km thickness constituted dominantly by garnet sillimanite gneiss-migmatite and garnet–clinopyroxene gneiss has been inferred in the Humboldt Mountains in CDML (Pant and Verma, 1994).

3. Petrography

3.1. Garnet–sillimanite gneiss

Garnet sillimanite gneiss is dominantly made up of quartz, garnet, sillimanite, K-feldspar and small amount of biotite, graphite and plagioclase. Two samples of this rock (CH51 and CH1) have been examined in detail. The major difference between the two is in the relative proportion of plagioclase + non-perthitic K feldspar (inferred to represent melt) which is significantly higher in CH51 (high melt) than CH1 (low melt). Thin section scale X-ray element maps of CH51 for Fe Kα, Al Kα, K Kα and Ca Kα (Fig. 2A–D) were obtained to understand the disposition and relative proportions of constituent minerals. Garnet is red coloured rounded poikiloblastic porphyroblasts in Fe Kα X-ray map (Fig. 2A) and constitute about 15% area of the thin section. These are embayed and anhedral, define a crude foliation and occur as refractory phase. Sillimanite occurring as red coloured prismatic grains in Al Kα X-ray maps (Fig. 2B) constitute ~10% to 12% of the thin section occurs along with garnet and graphite (Fig. 3A) and defines a strong alignment. Garnet and sillimanite show widely variable size with garnet grains up to 4 mm and sillimanite up to 2 mm in their maximum dimension. Fibrolite sillimanite occurs exclusively as inclusions in garnet and these garnets generally have overgrowths which are relatively inclusion free (Fig. 3B) indicating two-stage growth of garnet. Sporadically, sympletctitic biotite with quartz occurs close to the margins of garnet (Fig. 3C). Overall the rock contains low amount of biotite. K-feldspar is medium grained, anhedral to subhedral (1–4 mm) and is extensively present in this rock. It is observable as yellow and red coloured areas in K Ka X-ray map (Fig. 2C). It constitutes ~50% of the thin section area. It occurs in two textural modes, i.e. foliation defining (e.g. K Ka maps) and interstitial. Perthitic K-feldspar is anhedral (Fig. 3D) and it occurs with intergrowth of plagioclase and quartz with sporadic subhedral to euhedral non-perthitic K-feldspar (Fig. 3E). For computing the composition of perthitic K-feldspar two grains of perthites (Fig. 3G and H) were selected representing large variation of host versus exsolved phase. Areal proportion of the two in a single grain has been taken as the representative volumes of exsolved plagioclase and host K feldspar. Exsolved plagioclase varies from 4.9% to ~9% and the integrated compositions representing these are listed in Table 1 along with composition of the non-perthitic K feldspar. There are differences in composition of the perthitic K feldspar and non-perthitic K feldspar as former has higher Ca and Na and lower Ba than the latter. The non-perthitic K feldspars having a different composition and its association with quartz and plagioclase indicates it to be locally crystallized melt possibly as a result of biotite melting. It is thus inferred that there was no significant melt extraction. The green coloured, interstitial, relatively fine sized (0.1–0.4 mm) grains in Ca Kα X-ray map (Fig. 2D) represent the plagioclase and these occur in association with quartz and minor K-feldspar (Fig. 3D and E). Monazite has grown in association with the garnet overgrowth over fibrolite inclusion containing core (Fig. 3F).

3.2. Garnet–clinopyroxene gneiss (orthogneiss)

Major minerals in this rock are garnet, K-feldspar, clinopyroxene, calcic amphibole (hornblende), quartz and minor amounts of plagioclase. Garnet and green coloured clinopyroxene occur in textural equilibrium (Fig. 4A) and their smooth grain

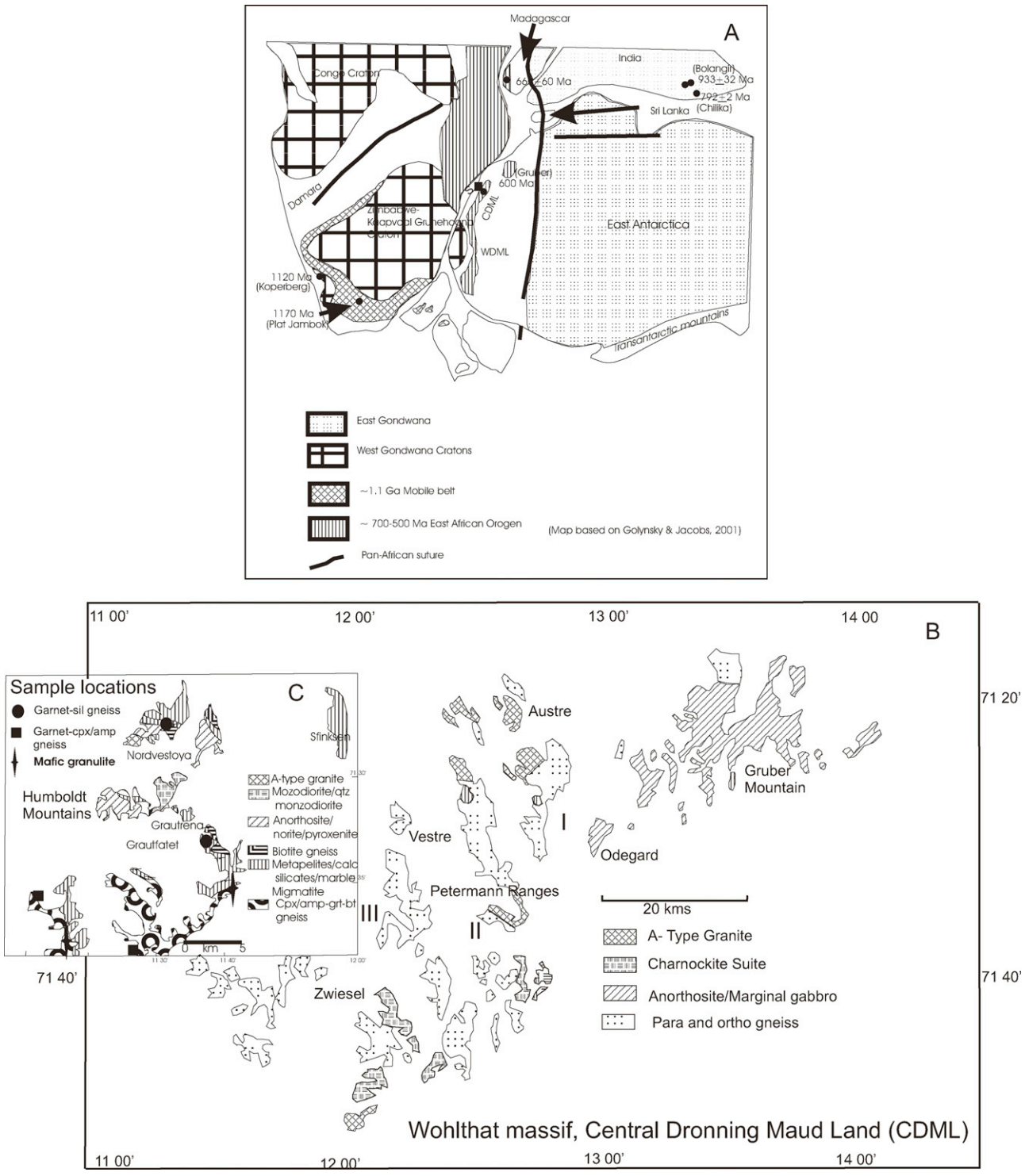

Fig. 1. (A) Regional map of a part of the reconstructed Gondwanaland (based on Golynsky and Jacobs, 2001) showing East African Orogen (EAO) and its possible extension in east Antarctica. Spot ages of massif anorthosite signifying anorogenic magmatism have been marked in this reconstruction and the EAO shows youngest episode of anorthosite magmatism. (B) In the Wohlthat Massif, Central Dronning Maud Land presence of extensive anorthosite, charnockite and A-type granite signifies anorogenic nature of Pan-African magmatism. Inset (C) is the geological map of the Humboldt Mountains. Note dominant occurrence of metapelites towards north and clinopyroxen/amphibole–garnet–biotite gneiss (granitic orthogneiss) towards south. Regional strike of the foliation is east–west and regional dips are towards south (CDML: Central Droning Maud Land; WDML: Western Dronning Maud Land; S: Schirmacher).

boundary contacts signify equilibrium and suitability for exchange geothermobarometry. Clinopyroxene is fine to medium grained (0.5–3 mm) and generally anhedral. Biotite occurs in variable proportions while apatite, zircon, magnetite, sphene are present as accessory minerals. Myrmekite is locally developed where microcline twinned K feldspar is abundant.

3.3. Mafic granulite

Mafic granulite occur parallel to the regional strike of the major S-surface. One of the mafic granulite is a two-pyroxene garnet granulite. Orthopyroxene is the dominant constituent with some grains occur as porphyroblasts (Fig. 4B) which have granulated margins

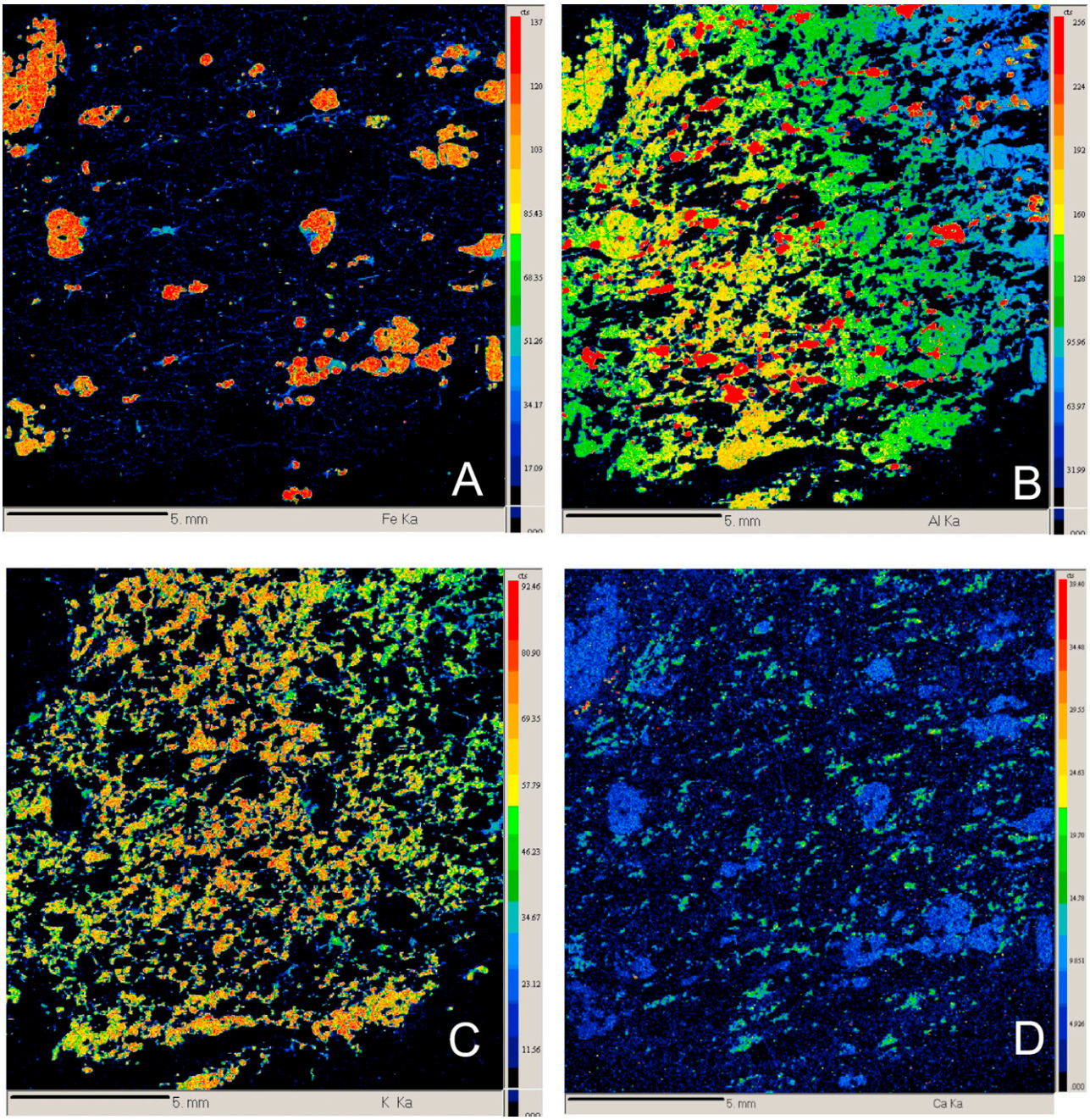

Fig. 2. Thin-section scale X-ray elemental map of garnet–sillimanite gneiss (CH-51, high melt). (A) Fe Kα map of the rock. Rounded, red coloured anhedral porphyroblasts represent garnet as the high Fe phase. Note poikiolblastic nature of garnets in the top left part. Light blue coloured domains adjacent to garnet are biotite. Garnets occur along foliation are anhedral. (B) Al Kα map of the thin section showing aligned nature of prismatic sillimanite marked in red colour. Some of the sillimanite are subhedral. Note the presence of red coloured patches in the top left cluster of garnets which is yellow coloured in this image (red coloured in A) indicating the presence of fibrolite inclusions. (C) K Kα map of the thin section. K feldspar, yellow and reddish-yellow coloured, constitutes the dominant phase in this rock. There is wide variability in the grain size with the smaller ones occurring as interstitial grains (left centre). High Fe and K (maps A and C) together indicates biotite and note that the rock contains very few biotite. (D) Ca Kα map of the thin section in which green coloured, interstitial grains are plagioclase and the violet coloured porphyroblasts are garnet. Note the relatively smaller size of plagioclase. It is mainly representative of melt fraction of this high melt garnet sillimanite gneiss. (For interpretation of the references to colour in this figure legend, the reader is referred to the web version of this article.)

indicating post formation deformation. Garnet is generally fine to medium grained and occurs interstially along with fine-sized clinopyroxene in textural equilibrium with both the pyroxenes. Amphiboles occur in two modes. Brown coloured matrix amphiboles occur associated with orthopyroxene and occasionally as inclusions in garnet (Fig. 4B). Secondary amphibole formed by the cleavage parallel hydration is also present in a large orthopyroxene porphyroblast (Fig. 4C).

4. Mineral chemistry

Representative mineral analyses are given in Tables 2 and 3. These include analyses from garnet–sillimanite gneiss, garnet–clinopyroxene (±hornblende) gneiss and mafic granulite.

The garnet in metapelites is dominantly Fe–Mg rich ($alm_{68}py_{28}$). The garnets are generally unzoned but rims of the large garnets show marginal Fe-enrichment ($alm_{73}py_{23}$) (Fig. 5A;

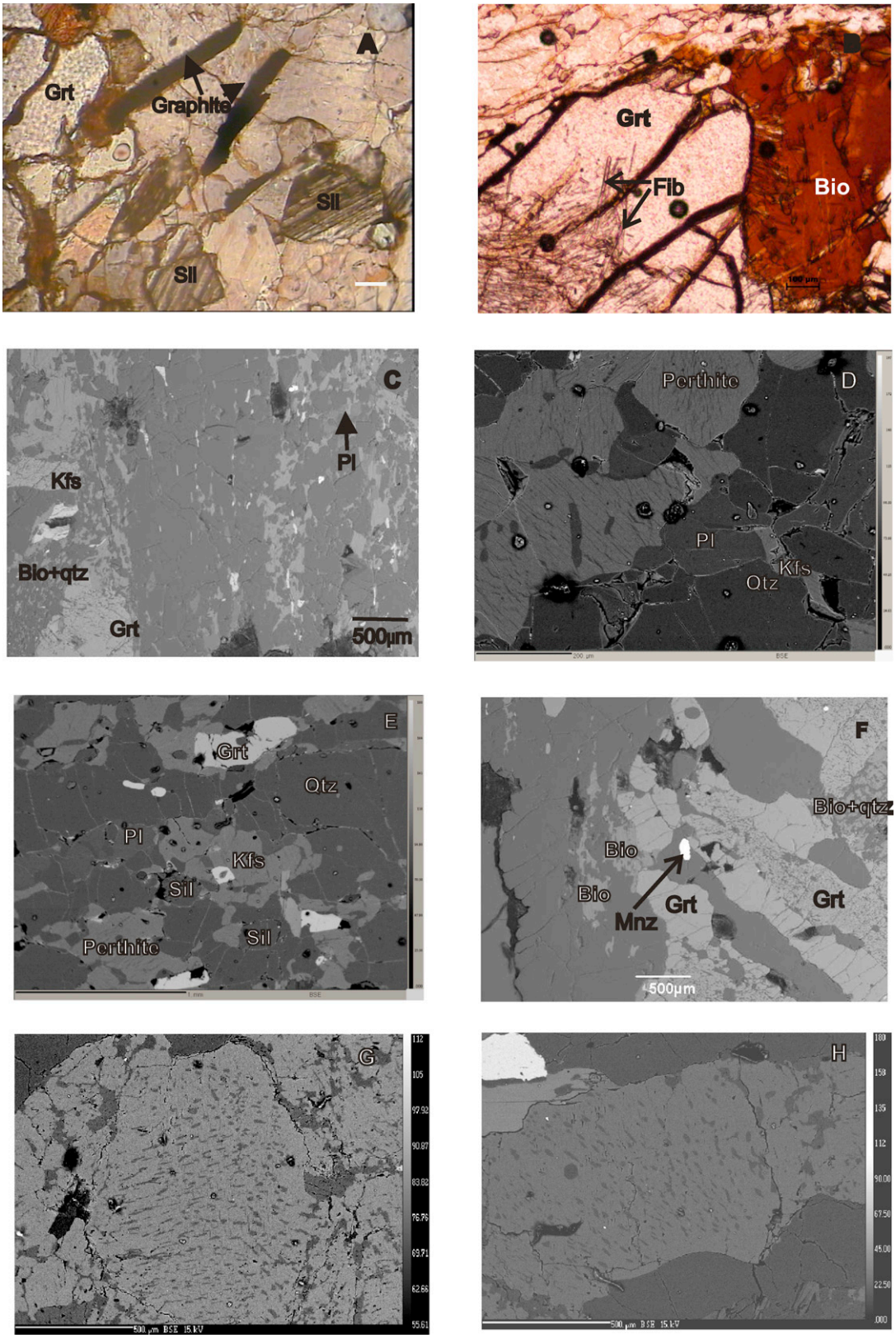

Fig. 3. Petrographic attributes of garnet–sillimanite gneiss. (A) Garnet–sillimanite–graphite in metapelitic granulite. Note diamond shaped cross sections of prismatic sillimante and black coloured flakes of graphite (PPL, bar scale 100 μm). (B) Photomicrograph of garnet–sillimanite gneiss (high melt). There is a distinct overgrowth of relatively inclusion free garnet over fibrolite bearing inner garnet. Biotite has smooth grain boundary contact with the outer garnet (PPL, bar scale 100 μm). (C) BSE image of garnet sillimanite gneiss (low melt) having biotite + quartz symplectitic intergrowth close to garnet rim. Perthitic K feldspar is present in the vicinity. Intermediate grey-tone, fine grained interstitial plagioclase (top-right) reflects low content of melt in this rock. (D) BSE image of high-melt garnet sillimanite gneiss. Note the presence of large mesoperthite along with quartz + plagioclase + non perthitic K feldspar which represents locally crystallized melt. (E) BSE image showing restitic garnet and sillimanite in a high melt domain within the garnet sillimanite gneiss. Note near absence of biotite in this field. Perthitic K feldspar represents a sub-solidus phase. Bar scale in the lower left margin is 1 mm. (F) BSE image of low melt garnet sillimanite gneiss. A large (~100 μm) matrix monazite is in textural equilibrium with garnet overgrowth (inclusion free)

Table 1
Composition of integrated perthitic K feldspar and K feldspar produced from biotite melting. Superscript refers to the two extreme percentages of proportions of exsolutions estimated from image analyses of perthites. Figures within brackets refer to number of analyses for averaging. Host Kfs is the composition of the K feldspar and exs that of the exsolution used for computing the integrated single feldspar compositon. Melt kfs refers to the composition of non-perthitic K feldspar inferred to be the in situ crystallized melt component.

	Perthitic K feldspar				Non-perthtic Kfeldspar
	exs ($n=3$)	Host Kfs	Integrated Kfs$^{4.9}$	Integrated Kfs^{9}	Melt Kfs ($n=4$)
SiO_2	62.68	63.32	63.29	63.26	64.06
Al_2O_3	22.57	18.15	18.36	18.54	18.27
TiO_2	0.01	0.05	0.05	0.04	0.02
Cr_2O_3	0.02	0.07	0.07	0.07	0.04
FeO	0.00	0.03	0.03	0.03	0.02
MnO	0.01	0.00	0.00	0.00	0.02
MgO	0.02	0.00	0.00	0.00	0.02
CaO	4.26	0.01	0.22	0.40	0.00
Na_2O	9.19	1.25	1.64	1.96	1.49
K_2O	0.17	14.97	14.24	13.64	14.01
P_2O_5	0.11	0.16	0.16	0.15	0.10
BaO	0.09	0.01	0.01	0.01	0.44
F	0.00	0.00	0.00	0.00	0.17
Cl	0.00	0.01	0.01	0.01	0.01
Total	99.13	98.03	98.08	98.13	98.67

supplementary table 1A). The grossular content of the garnets is low (2–3 mol%) and spessartine is insignificant. Garnet in the orthogneiss (garnet–clinopyroxene gneiss) is Fe–Ca rich ($alm_{69}grs_{26}$) with pyrope molecule ~5 mol%. In contrast to these, garnets of the mafic granulite are solid solution of three end members ($alm_{58}py_{22}grs_{18}$). These are generally unzoned (Fig. 5B; supplementary table 1B). Clinopyroxene has been analysed in garnet–clinopyroxene gneiss as well as mafic granulite. Clinopyroxene in mafic granulite is more magnesian and calcic ($wo_{54}en_{39}fs_{12}$) than in the garnet–clinopyroxene gneiss in which it is Fe-enriched ($wo_{45}en_{16}fs_{39}$) while orthopyroxene in the mafic granulite has intermediate composition ($wo_1en_{56}fs_{43}$). Orthopyroxene in mafic granulite is unzoned (Fig. 5C; supplementary table 1C). Amphibole occurring as inclusion in garnet and in matrix is magnesiohornblende (Table 2; nomenclature following Leake et al., 1997).

Biotite content of the metapelites is generally low and whenever present it is high titanium (TiO_2 ~4%) and magnesian (Fe/Fe + Mg ~ 0.37).

5. Metamorphic evolution

5.1. Metapelites

Preservation of folded fibrolite trails within garnets can be explained by the first formation of sillimanite possibly from kyanite by the following discontinuous reaction:

$$\text{Kyanite} = \text{sillimanite} \quad (R1)$$

Prismatic blades of sillimanite occur in the matrix where the dominant K-bearing phase is perthitic as well as non-perthitic K-feldspar and it marks the second sillimanite isograde. The simplest reaction for this assemblage can be;

$$\text{Muscovite} + \text{quartz} = \text{K-feldspar} + \text{sillimanite} + H_2O \quad (R2)$$

This reaction has been experimentally investigated (Helgeson et al., 1978) and the univariant curve indicates a temperature of 740 °C at ~6 kbar pressure. Oriented fibrolite occurs as inclusions in garnet (Fig. 3F). Fibrolite can form both from mica as well as from polymorphic transformation of aluminosilicates but there is practically no biotite inclusion in garnet. Kyanite (and andalusite) to sillimanite phase transformation to fibrolite can occur as a consequence of deformation (Goergen et al., 2008). There is also some evidence that fibrolite forms at 50–80 °C lower temperature than prismatic sillimanite (Larson and Zachary, 2001) which is consistent with its occurrence as a prograde phase in the garnet sillimanite gneiss where prismatic sillimanite occurs associated with perthitic K feldspar and the latter association can be well explained by the muscovite breakdown reaction.

On the other hand, low to very low concentrations of biotite and the presence of garnet with melt in form of plagioclase + K feldspar + quartz indicates biotite melting reaction to have taken place in the garnet sillimanite gneiss of the Humboldt Mountains.

$$\text{Biotite} + \text{plagioclase} + \text{quartz} = \text{garnet} + \text{K-feldspar} + \text{melt} \quad (R3)$$

This biotite melting reaction in the NCKFMASH system appears to have been operative as generally cordierite and orthopyroxenes are not present in the assemblages. However, whatever biotite is present has high titanium (~4% TiO_2), rutile is present as a stable phase in the assemblage and ilmenite is also present often as inclusion in the garnet and the biotite melting may have been more complex than (R3) in form of following reaction:

$$\text{Biotite} + \text{ilmenite} + \text{plagioclase} + \text{quartz} = \text{garnet} + \text{K-feldspar} + \text{rutile} + \text{melt} \quad (R4)$$

Grew (1981) studied garnet sillimanite gneiss from Molodezhnaya Station which is ~80 km north of the Humboldt Mountains and indicated 700 °C and 5.5 ± 1 kbar as the metamorphic conditions for these assemblages. He used semi-quantitative μH_2O–μCO_2 plots to show that garnet + biotite + sillimanite association is produced at higher μH_2O and lower P_{H_2O} than garnet + biotite + cordierite and this is reflected in the biotite composition which contains fluorine (~0.5–1%) besides high Ti.

Fibrolite filled inner garnet having inclusion free overgrowth implies two stage growth of the garnet. The embayed nature of these grains indicates their resorption at some stage of the growth. These metapelitic granulites contain restitic sillimanite + perthite ± garnet assemblage interspersed with melt represented by non-perthitic K feldspar + quartz ± plagioclase

over the fibrolite containing garnet. Note higher proportion of matrix biotite in the low melt garnet sillimanite gneiss. (G and H) BSE images of perthites used for computing the integrated composition by area calculation of host and exsolution. The two perthite grains represent the variability of proportion of exsolution plagioclase between 9% and 4.9% (mineral abbreviations: Grt: garnet; Kfs: Kfeldspar; Sil: sillimanite; qtz: quartz; Pl: plagioclase; Mnz: monazite).

Table 2
Analyses of representative minerals in garent–sillimanite gneiss, Humboldt Mountains, Central Dronning Maud Land, East Antarctica.

Mineral	Garnet						Sillimanite		Biotite			Perthite				Plagioclase			Ilmenite		Rutile
Comment	SC	SR	SR	SC	BC	BR	M					AL	KH	AL	KH	C	I	R			
Dataset	3/1	4/1	6/1	8/1	28/1	29/1	1/1		30/1	31/1	32/1	19/1	20/1	26/1	27/1	23/1	24/1	25/1	9/1	13/1	10/1
SiO_2	38.932	38.495	38.486	38.356	38.859	38.282	37.514		37.95	37.85	39.25	66.52	64.82	67.28	65.69	65.47	65.40	67.28	0.06	0.02	0.05
TiO2	0.023	0	0	0.165	0	0	0.066		4.07	3.81	3.76	0.00	0.00	0.00	0.00	0.01	0.00	0.04	50.14	51.53	97.88
Al_2O_3	21.339	21.547	21.659	21.596	21.537	21.235	62.45		17.37	17.77	17.34	21.62	18.46	21.54	18.59	22.51	22.05	20.24	0.05	0.08	0.05
Cr_2O_3	0.076	0.018	0	0.102	0	0.008	0.039		0.05	0.05	0.00	0.02	0.00	0.07	0.05	0.00	0.01	0.12	0.12	0.19	0.06
FeO	31.681	31.311	32.079	31.553	31.246	33.989	0.161		13.75	13.63	12.26	0.07	0.00	0.03	0.07	0.00	0.00	0.05	45.47	44.39	0.07
MnO	0.152	0.234	0.229	0.216	0.273	0.242	0.052		0.06	0.04	0.01	0.00	0.02	0.01	0.00	0.04	0.00	0.00	0.23	0.03	0.00
MgO	7.37	7.209	7.193	7.574	7.521	5.994	0.065		12.41	12.24	12.22	0.01	0.02	0.03	0.00	0.00	0.00	0.11	0.84	1.24	0.06
CaO	1.405	0.86	0.777	1.365	1.081	0.971	0.022		0.06	0.03	0.10	2.63	0.00	2.58	0.00	3.62	3.28	0.75	0.03	0.03	0.00
Na_2O	0.001	0	0	0.039	0	0	0.057		0.12	0.16	0.19	10.53	0.94	10.29	1.63	9.80	9.99	11.21	0.06	0.00	0.03
K_2O	0.003	0	0	0.007	0.019	0.002	0.007		8.99	8.94	8.64	0.07	15.35	0.05	14.67	0.12	0.14	0.14	0.00	0.01	0.00
Total	101.269	100.12	100.674	101.118	100.659	101.01	100.495		95.17	95.18	94.56	101.55	99.96	102.24	101.24	101.70	101.01	100.10	96.99	97.51	98.21
Oxygen	12	12	12	12	12	12	5		12	12	12	8	8	8	8	8	8	8	3	3	
Si	3.017	3.016	3.002	2.977	3.017	3.008	1.009		3.061	3.059	3.159	2.886	2.997	2.901	2.998	2.843	2.858	2.949	0.001	0.000	
Ti	0.001	0.000	0.000	0.010	0.000	0.000	0.001		0.247	0.232	0.228	0.000	0.000	0.000	0.000	0.000	0.000	0.001	0.981	0.994	
Al	1.949	1.990	1.991	1.975	1.971	1.966	1.979		1.651	1.693	1.645	1.105	1.006	1.094	1.000	1.152	1.136	1.046	0.001	0.002	
Cr	0.005	0.001	0.000	0.006	0.000	0.000	0.001		0.003	0.003	0.000	0.001	0.000	0.003	0.002	0.000	0.000	0.004	0.003	0.004	
Fe + 3	0.000	0.000	0.000	0.000	0.000	0.000	0.000		0.000	0.000	0.000	0.000	0.000	0.000	0.000	0.000	0.000	0.000	0.000	0.000	
Fe + 2	2.053	2.052	2.093	2.048	2.029	2.234	0.004		0.928	0.921	0.825	0.002	0.000	0.001	0.003	0.000	0.000	0.002	0.989	0.952	
Mn	0.010	0.016	0.015	0.014	0.018	0.016	0.001		0.004	0.003	0.001	0.000	0.001	0.000	0.000	0.001	0.000	0.000	0.005	0.001	
Mg	0.852	0.842	0.836	0.876	0.871	0.702	0.003		1.492	1.475	1.466	0.001	0.001	0.002	0.000	0.000	0.000	0.007	0.033	0.047	
Ca	0.117	0.072	0.065	0.114	0.090	0.082	0.001		0.005	0.003	0.009	0.122	0.000	0.119	0.000	0.169	0.154	0.035	0.001	0.001	
Na	0.000	0.000	0.000	0.006	0.000	0.000	0.003		0.019	0.026	0.030	0.886	0.085	0.860	0.144	0.825	0.846	0.953	0.003	0.000	
K	0.000	0.000	0.000	0.001	0.002	0.000	0.000		0.925	0.922	0.887	0.004	0.905	0.003	0.854	0.006	0.008	0.008	0.000	0.000	
Total	8.005	7.988	8.002	8.026	7.998	8.009	3.001		8.336	8.335	8.249		5.006	4.995	4.982	5.000	4.997	5.001	5.005	2.017	2.002
Alm	67.73	68.82	69.54	67.10	67.47	73.63		Fe*	0.38	0.38	0.36	Ab	87.54	8.54	87.57	14.42	82.50	84.00	95.65		
Py	28.09	28.24	27.80	28.71	28.95	23.15						An	12.09	0.00	12.14	0.00	16.85	15.24	3.54		
Grs	3.85	2.42	2.16	3.72	2.99	2.69						Or	0.36	91.46	0.29	85.58	0.65	0.76	0.81		
Sp	0.33	0.52	0.50	0.47	0.60	0.53															

Explanation for abbreviations: Fe* = Fe^{2+}/Fe^{2+} + Mg, S: small, R: rim, B: big, C: core, I: intermediate, M: matrix, A: albite, K: k-feldspar, L: lamillae, H: host. Biotite contains in the addition 0.1–0.5 wt.% F. K-feldspar host has 0–0.35 wt.% BaO.

Table 3
Representative mineral chemistry of orthopyroxene, clinopyroxene, garnet, amphibole and plagioclase in mafic granulite and garnet–clinopyroxene gneiss.

	Mafic granulite											
	Orthopyroxene					Clinopyroxene		Garnet		Amphibole	Plagioclase	
Dataset/point	1/1	3/1	4/1	6/1	7/1	2/1		8/1	11/1		1	2
SiO_2	51.99	51.91	52.08	52.34	52.02	52.81		38.72	38.66	44.57	48.67	49.24
TiO2	0.03	0.10	0.09	0.00	0.17	0.18		0.00	0.13	2.03	0	0
Al_2O_3	1.70	1.56	0.61	1.25	1.54	1.79		21.14	21.01	11.61	32.79	32.63
Cr_2O_3	0.07	0.08	0.02	0.05	0.08	0.01		0.08	0.00	0.09	0	0
FeO	26.40	26.50	26.76	26.47	25.69	8.46		27.30	26.59	10.3	0	0
MnO	0.27	0.28	0.31	0.20	0.13	0.05		0.74	0.53	0	0	0
MgO	19.31	19.45	19.66	19.43	19.50	13.43		5.45	5.91	13.49	0	0
CaO	0.57	0.41	0.36	1.09	1.25	23.85		6.49	6.95	12.21	16.36	16.07
Na_2O	0.05	0.01	0.01	0.06	0.02	0.30		0.03	0.04	1.06	2.17	2.13
K_2O	0.02	0.00	0.00	0.00	0.00	0.00		0.00	0.00	1.4	0.03	0.09
Total	100.40	100.30	99.89	100.89	100.39	100.87		99.94	99.81	96.76	100.02	100.16
Oxygen	6	6	6	6	6	6		12	12	23	8	8
Si	1.964	1.964	1.979	1.968	1.962	1.950		3.028	3.018	6.542	2.225	2.244
Ti	0.001	0.003	0.002	0.000	0.005	0.005		0.000	0.008	0.224	0	0
Al	0.076	0.070	0.027	0.055	0.068	0.078		1.948	1.933	2.008	1.767	1.753
Fe + 3	0.000	0.000	0.009	0.013	0.000	0.034		0.000	0.000	0.041	0	0
Cr + 3	0.002	0.002	0.001	0.002	0.002	0.000		0.005	0.005	0.01	0	0
Fe + 2	0.834	0.838	0.842	0.820	0.810	0.227		1.785	1.736	1.222	0	0
Mn	0.009	0.009	0.010	0.006	0.004	0.002		0.049	0.035	0	0	0
Mg	1.087	1.097	1.114	1.089	1.096	0.739		0.635	0.687	2.952	0	0
Ca	0.023	0.016	0.015	0.044	0.050	0.944		0.544	0.581	1.92	0.801	0.785
Na	0.003	0.001	0.001	0.004	0.001	0.022		0.004	0.006	0.299	0.193	0.188
K	0.001	0.000	0.000	0.000	0.000	0.000		0.000	0.000	0.262	0.002	0.005
Total	4.000	4.000	4.000	4.000	4.000	4.000		7.998	8.009	15.480	4.988	4.975
Wo	1	1	1	2	3	49	Alm	0.593	0.571			
En	56	56	57	56	56	39	Py	0.211	0.226	Ab	0.19	0.19
Fs	43	43	43	42	41	12	Gros	0.180	0.191	An	0.80	0.80
XFe	0.43	0.43	0.43	0.43	0.42	0.24	Sp	0.016	0.011	Or	0.00	0.01

	Garnet–clinopyroxene gneiss					
	Clinopyroxene			Garnet		Plagioclase
	Core	Rim		Core	Rim	
	1	2		3	4	5
SiO_2	48.79	48.66		37.54	38.22	61.17
TiO2	0.34	0.3		0	0	0.01
Al_2O_3	2.55	2.27		20.87	20.71	23.39
Cr_2O_3	0.01	0		0	0	0
FeO	22.27	22.39		32.05	30.16	0.04
MnO	0.22	0.06		0.69	0.69	0
MgO	5.01	5.12		1.52	1.31	0.5
CaO	20.79	21.14		8.88	10.19	8.26
Na_2O	0.7	0.6		0	0	5.73
K_2O				0	0	0.28
Total	100.68	100.54		101.55	101.28	99.38
Oxygen	6	6		12	12	8
Si	1.928	1.928		2.966	3	2.747
Ti	0.01	0.009		0	0	0
Al	0.119	0.106		1.937	1.919	1.238
Fe + 3	0	0		0	0	0.002
Cr + 3	0	0		0	0	0
Fe + 2	0.736	0.742		2.18	2.05	0
Mn	0.007	0.002		0.046	0.046	0
Mg	0.295	0.303		0.179	0.153	0.003
Ca	0.88	0.897		0.751	0.859	0.276
Na	0.053	0.046		0	0	0.719
K	0	0		0	0	0.016
Total	4.028	4.033		20.059	20.027	5.001
Wo	46	46	Alm	0.69	0.66	Ab 0.71
Fs	39	38	Py	0.06	0.05	An 0.27
En	15	16	Grs	0.24	0.28	Or 0.02
			Sp	0.01	0.01	

produced by dehydration melting of biotite as is common in granulite facies terrain (Fyfe, 1970; Thompson, 1982). Such in situ crystallization and low-melt extraction leads to some degree of back reactions between the melt and the restite (Kriegsman and Hensen, 1998) causing partial reversal of the reaction such as (R3) and (R4). The textural imprint of this reversal will result in embayed garnets and quartz + biotite ± plagioclase growth which are evident in garnet sillimanite gneiss (Fig. 3C and F).

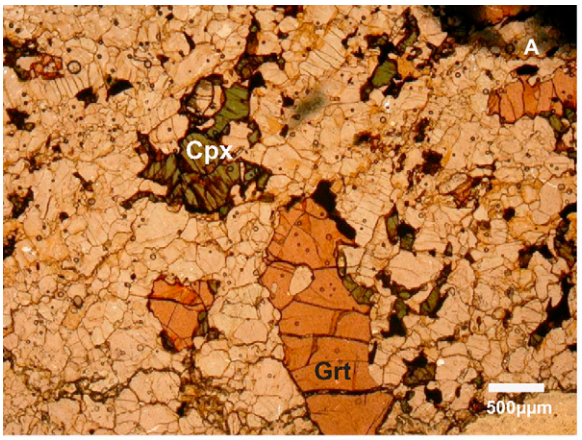

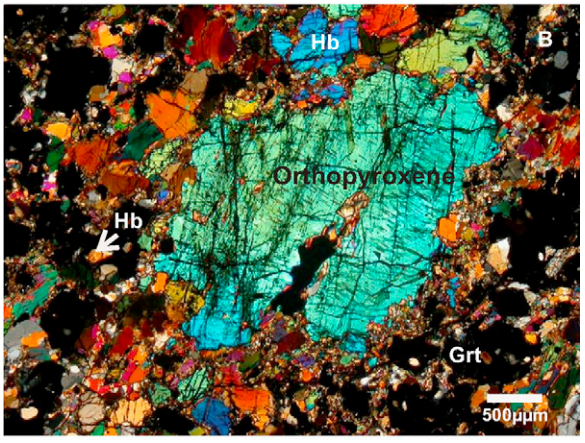

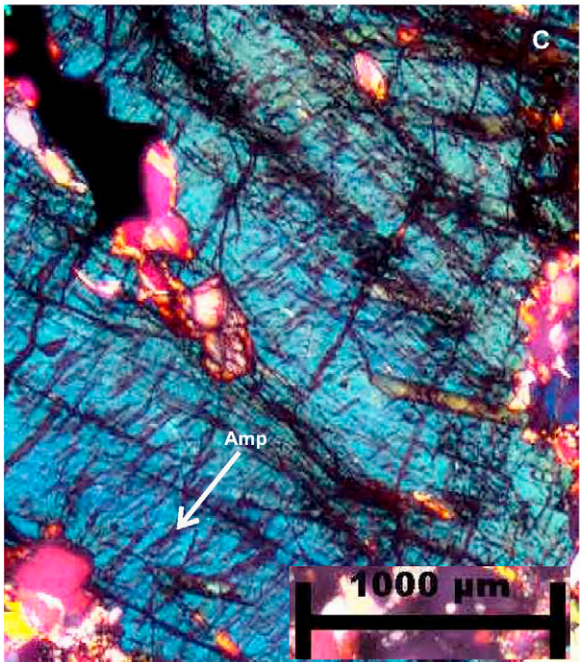

Fig. 4. (A) Photomicrograph of garnet–clinopyroxene gneiss under plane polarized light. Note smooth grain boundary contact between garnet and clinopyroxene (cpx). The clinopyroxene is hedenbergite (plane polarized light). (B) Photomicrograph of mafic granulite under crossed nicols. Note large orthopyroxene porphyroblast with granulated margins. Garnet is generally smaller and clinopyroxene content is low. Hornblende (Hb) is present in matrix as well as inclusion in garnet. (C) Enlarged view of the large orthopyroxene of (B) (under crossed nicols) showing formation of amphiboles along cleavages by hydration (other mineral abbreviations as in Fig. 3).

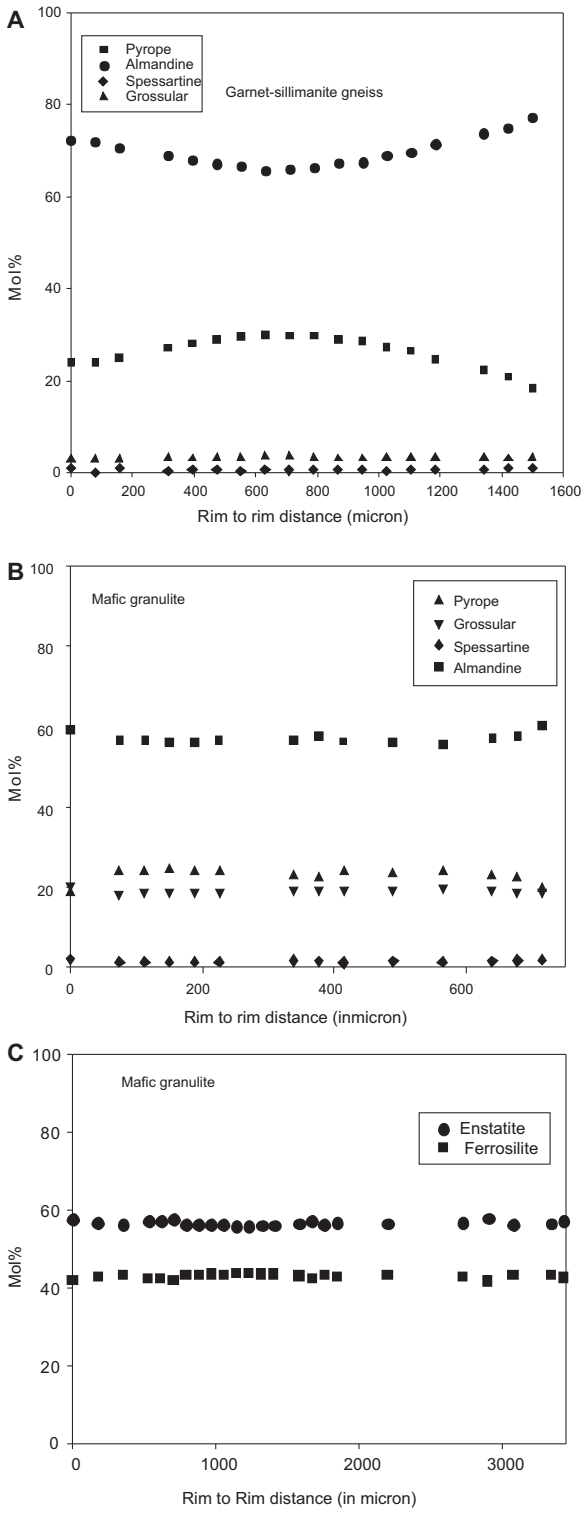

Fig. 5. (A) Rim to rim zoning profile of a ~1.6 mm garnet in garnet sillimanite gneiss. Garnet is dominantly made up of almandine and pyrope and shows a very broad, symmetrical zoning in form of marginal Fe enrichment at the rims. (B) Rim to rim zoning profile of a garnet in mafic granulite. This garnet is made up of almandine, pyrope and grossular with pyrope and grossular present in comparable proportion. The garnet is nearly unzonce. (C) Rim to rim zoning profile of a large (~4 mm) orthopyroxene from mafic granulite. Note nealy unzoned nature of the orthopyroxene.

5.2. Mafic granulites

Transition of amphibolite to granulite in mafic rocks is marked first by appearance of clinopyroxene and than at still high temperature by the appearance of orthopyroxene well over 800 °C (Spear, 1981) but the temperature is lowered by ~50 °C if quartz is present (Binns, 1968; Spear, 1981). The mafic granulite is dominantly made up of orthopyroxene, garnet, hornblende, plagioclase, quartz and clinpyroxene. The garnet + clinopyroxene assemblage formed by the following reaction:

$$\text{Fe-hornblende} + \text{quartz} = \text{garnet} + \text{clinopyroxene} + \text{plagioclase} \quad \text{(R5)}$$

At higher temperature than for R5, orthopyroxene is likely to have formed by common sliding reaction:

$$\text{Hornblende} + \text{almandine} + \text{quartz} = \text{orthopyroxene} + \text{plagioclase} + H_2O \quad \text{(R6)}$$

The presence of garnet implies a Fe-enriched bulk for the mafic protolith.

6. P–T conditions of metamorphism

The conditions of metamorphism have been estimated by conventional geothermobarometry as well as by pseudosection analyses of garnet sillimanite gneiss and garnet clinopyroxene gneiss. In garnet sillimanite gneiss, core garnet and biotite temperatures are ~700 ± 50 °C while the rim temperatures are ~70 °C lower possibly reflecting cooling related diffusion (Table 4A). The pressure estimates using garnet–plagioclase–quartz–sillimanite (GOPS) geobarometry are 6.3 ± 0.9 kbar for core and 5.3 ± 1.1 kbar for rim garnet composition. The presence of rutile and ilmenite in the assemblage allows estimation of pressure using garnet–rutile–ilmenite–plagioclase–sillimanite and garnet–rutile–ilmenite–sillimanite calibrations which indicate a pressure of 6–7 kbar which is in agreement with the GOPS geobarometry. Using Fe–Mg exchange geothermometry highest temperatures of ~850 °C are obtained from the mafic granulite for orthopyroxene–clinopyroxene pair and the rim temperatures are similar (Table 4B). Garnet–clinopyroxene Fe–Mg exchange records lowest temperatures (612 ± 64 °C for core and 584 ± 66 °C for rim) in mafic granulite and this is within the range of the rim temperature of the garnet–sillimanite gneiss. However there is no significant difference in core and rim temperatures in multiple exchange geothermometric mineral pairs in mafic granulite which is in corroboration with their chemically unzoned nature (Fig. 5A–C). Garnet–clinopyroxene gneiss shows temperatures of 794 ± 60 °C for Fe–Mg exchange of core compositions of coexisting garnet and hedenbergite and rim temperatures of 775 ± 73 °C in a manner similar to the mafic granulite (Table 4B). The pressure estimates vary between 5 and 8 kbar and a peak pressure of ~8 kbar is indicated. Thus, in summary peak temperature attained by these low to intermediate pressure granulites is 800–850 °C and it is best preserved in mafic granulite. Core and rim P–T conditions in the garnet–sillimanite gneiss records evidence of diffusion related cooling along with a pressure drop of ~1 kbar.

For pseudosection calculations garnet–sillimanite gneiss with neo-crystallized plagioclase + quartz + K-feldspar (melt) and garnet–clinopyroxene gneiss having garnet + hedenbergite + K feldspar + plagioclase + quartz assemblage was selected. X-ray Fluorescence analyses of representative samples (analyses carried out at the laboratories of Airborne Mineral Survey Exploration wing of Geological Survey of India) were used and the weight percent

Table 4A
Geothermobarometry from garnet–sillimanite gneiss.

	Geothermometry									Geobarometry					
	Fe–Mg exchange (Grt-bio)									gar-plag-q-sil				GRAIL	GRIPS
	T	GA	HL	FS	LP	HS	PL	P	IM	WG	B	KN	K	HC	GS	NH	B	BL
C (LG)	710	705	680	706	680	738	751	667	611	750	606	6275	7065	5662	5310	5273	6165	6504
R (LG)	617	586	601	612	617	623	619	604	501	627	553							
C (SG)	723	732	691	756	689	772	691	680	630	773	615	7246	7968	5549	6419	6252	6003	6986
R (SG)	688	667	661	707	666	716	668	648	580	714	591	5960	6830	4009	4591	4943	6399	6472

T: Thompson (1976), GA: Goldman and Albee (1977), HL: Holdaway and Lee (1977), FS: Ferry and Spear (1978), LP: Lavrent'eva and Perchuk (1981), HS: Hodges and Spear (1982), PL: Perchuk and Lavrent'eva (1983), P: Perchuk et al. (1985), IM: Indares and Martignole (1985), WG: Williams and Grambling, 1990, B: Bhattacharya et al. (1992), KN: Koziol and Newton (1988), K: Koziol (1989), Hodges and Crowley (1985), Ganguly and Saxena (1984), Newton and Haselton (1981), Bohlen et al. (1983), Bohlen and Liotta (1986); C(LG): core large garnet, R(LG): rim large garnet, C(SG): core small garnet, R (SG): rim small garnet.
Temperature: garnet core-biotite 698 + 50 °C; garnet rim-biotite 630 + 53 °C; pressure: GOPS core 6.3 + 0.9 kbar and rim −5.3 + 1.1 kbar.

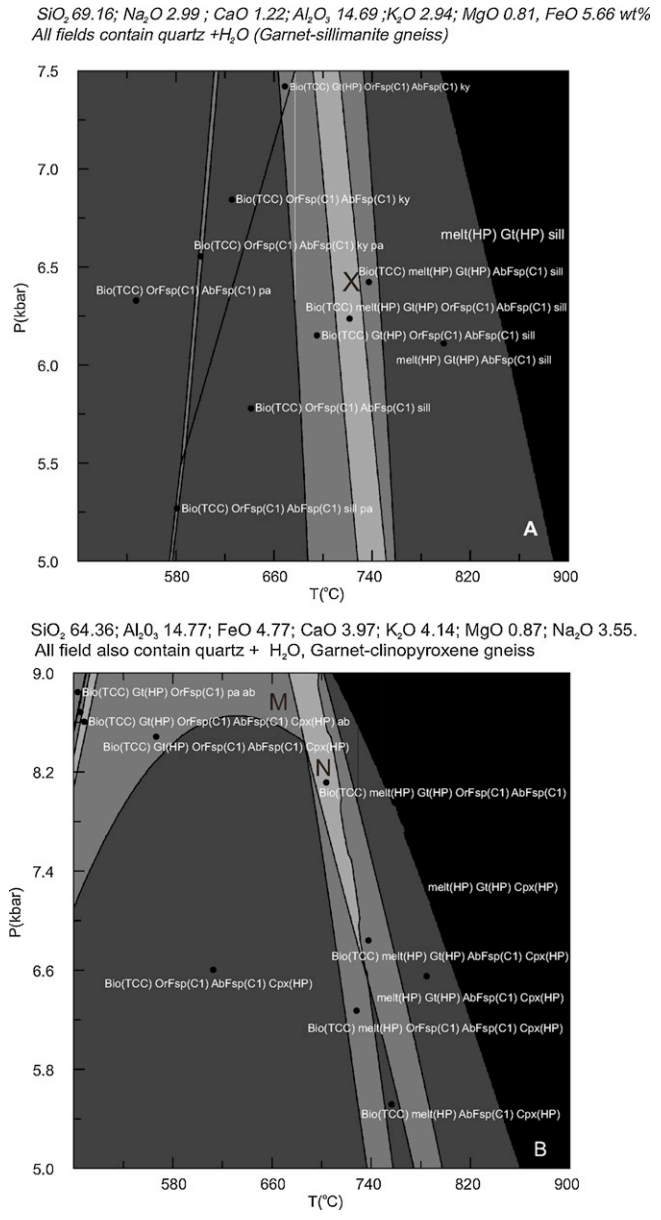

Fig. 6. (A and B) NCKFMASH pseudosection computed for garnet sillimanite gneiss (sample no. 26) and garnet–clinopyroxene gneiss (sample no. 65) from the Humboldt Mountains, CDML, East Antarctica (explanation in text). Solution models (HP: Holland and Powell, 1998); biotite (TCC: Tajcmanova et al., 2009); silicate melt (HP: Holland and Powell, 1998); ternary feldspar (Holland and Powell, 2003; AbFsP, OrFsP and Pl (C1) Van Laar versions; AbFsp(C1) and OrFsp(C1) represent alkali feldspar solid solutions with C1 structural state); clinopyroxene (Holland and Powell, 1998) (other mineral abbreviations: bio: biotite; gt: garnet; sill: sillimanite; pa: paragonite; ky: kyanite; cpx: clinopyroxene).

oxide analyses are indicated in the constructed pseudosections (Fig. 6A and B).

The pseudosection presented in this study was calculated based on the Gibbs free energy minimization concept of Connolly (1990) (Perple_X 07 version). The internally consistent thermodynamic data set and equation of state for H_2O Holland and Powell (1998 and revised 2003) was used for calculations. Garnet, anorthite, potash feldspar, biotite, sillimanite, kyanite, paragonite, clinopyroxene were considered for the pseudosection calculation. The following solid solution models were used in the calculations Garnet (HP: Holland and Powell, 1998); biotite (TCC: Tajcmanova et al., 2009); silicate melt (HP: Holland and Powell, 1998); ternary

Table 4B
Geothermometric and geobarometric data for sample of mafic granulite and garnet–clinopyroxene gneiss.

Opx	Cpx	Garnet			Plagioclase	Temterature (°C)								Cpx-Opx			Grt-Opx	Pressure (kbar)							
						Grt-Cpx												Grt-Opx-Plag						Grt-Cpx-Pl	
XFe	XFe	XFe	XMg	XCa	XAn	MH	RG	MG	EG	G	D	P	K	PTN	S	WB	NW	BM	D	H	PC	PAN	E	PH	E
																					Fe	Mg			
Mafic granulite																									
	0.24	0.57	0.23	0.19		553	579	550	616	734	545	594	547	490	630										
	0.24	0.59	0.21	0.18		584	599	576	648	758	577	627	586	517	646										
0.43	0.24															748	824	852							
0.42	0.24															750	830	852							
0.43		0.57	0.23	0.19	0.803														700	640	7.83	8.12	5.76	5.44	
0.43		0.57	0.23	0.19	0.083														689	634	7.85	8.26	5.77	5.45	
0.42		0.57	0.23	0.19															673	625					
0.43		0.59	0.21	0.18	0.803																8.34	8.18	6.42	6.1	
0.43		0.59	0.21	0.18	0.804																8.21	8.13	6.3	5.98	
0.43	0.24	0.57	0.23	0.19	0.804														686	633					4.26 4.87
	0.24	0.59	0.21	0.18	0.803																				5 5.58
Garnet–clinopyroxene gneiss (orthogneiss)																									
C	0.71	0.69	0.06	0.24		773	715	736	827	894		812	800												
R	0.71	0.66	0.05	0.28		725	687	696	825	878		811	804												

MH: Mysen and Heier (1972), RG: Raheim and Green (1974), MG: Mori and Green (1978), EG: Ellis and Green (1979), G: Ganguly (1979), D: Dahl (1980), P: Powell (1985), K: Krogh (1988), PTN: Pattison and Newton (1989), S: Sengupta et al. (1989), WB: Wood and Bano (1973), NW: Nehru and Wyllie (1974), BM: Bertrand and Mercier (1985), H: Harley (1984a,b), PC: Perkins and Chipera (1985), PH: Powell and Holland (1988), E: Eckert et al. (1991), PAN: Perkins and Newton (1981), Newton and Perkins (1982).
Garnet–clinopyroxene geothermometer – Garnet–clinopyroxene gneiss: Core 794 ± 60 °C; rim 775 ± °C; mafic granulite: core 612 + 64 °C; Rim 584 + 66 °C.

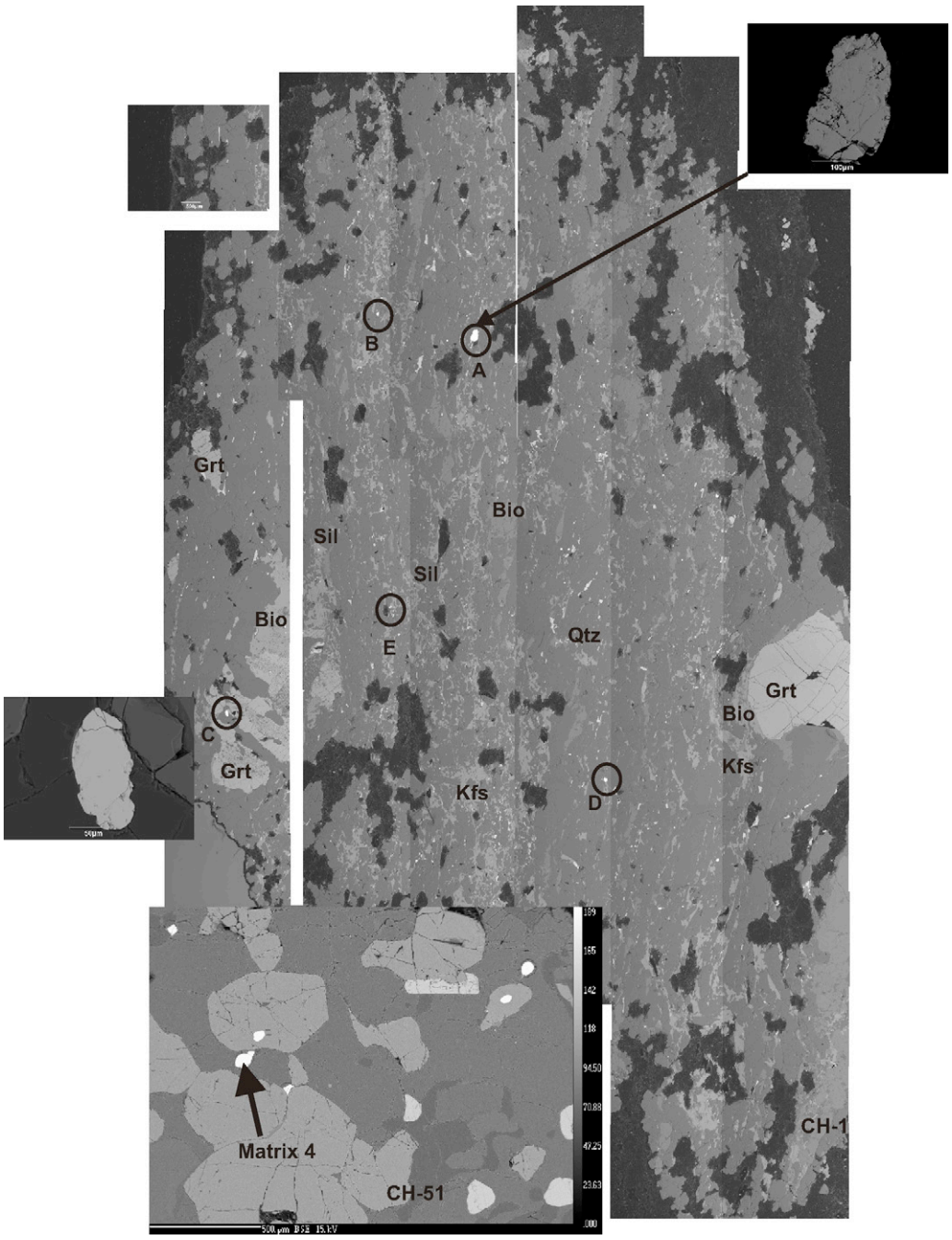

Fig. 7. Back scattered electron (BSE) composite map of low-melt garnet sillimanite gneiss showing the locations of monazites. Blown up BSE images of two analysed matrix grains A and C are also shown. For scale of this composite thin section map, an image with scale is given at top-left. Note higher proportion of biotite compared to the high melt garnet sillimanite gneiss (Fig. 2). The inset in the lower half is a BSE image of high melt garnet sillimanite gneiss with matrix monazite grain 4 for comparison. Note near absence of biotite and dominant presence of plagioclase and quartz.

feldspar (Holland and Powell, 2003; AbFsP, OrFsP and Pl (C1) Van Laar versions); clinopyroxene (Holland and Powell, 1998). Plagioclase exsolution in perthite has ~12 mol% anorthite content in this rock indicating the ternary nature of feldspar solid solution (Table 2). In view of this the ternary feldspar solid solution model was chosen for pseudosection computation. AbFsp(C1) and OrFsp(C1) represent alkali feldspar solid solutions with C1 structural state. In both the samples water and the quartz were treated as saturated components.

In garnet sillimanite gneiss, garnet + sillimanite + K feldspar (solid solution) + melt ± biotite assemblage is stable in a narrow pressure independent field (field X in Fig. 6A) and limits the temperature of the assemblage to 720–730 °C which is in reasonable agreement with the temperatures obtained by Fe–Mg exchange thermometry. Garnet + clinopyroxene + K feldspar + plagioclase + biotite assemblage is stable at relatively higher pressure (>7.5 kbar; Field M in Fig. 6B) between 600 and 700 °C and the same association with melt occurs at temperatures in excess of 700 °C at lower pressures (Fields N; Fig. 6B). This is in conformity with the observed assemblage and garnet–clinopyroxene Fe–Mg exchange geothermometry within the error bars of estimated temperatures (Table 3B). Thus, there is in general a good agreement between estimates of P and T using conventional geothermobarometry and pseudosection analyses for

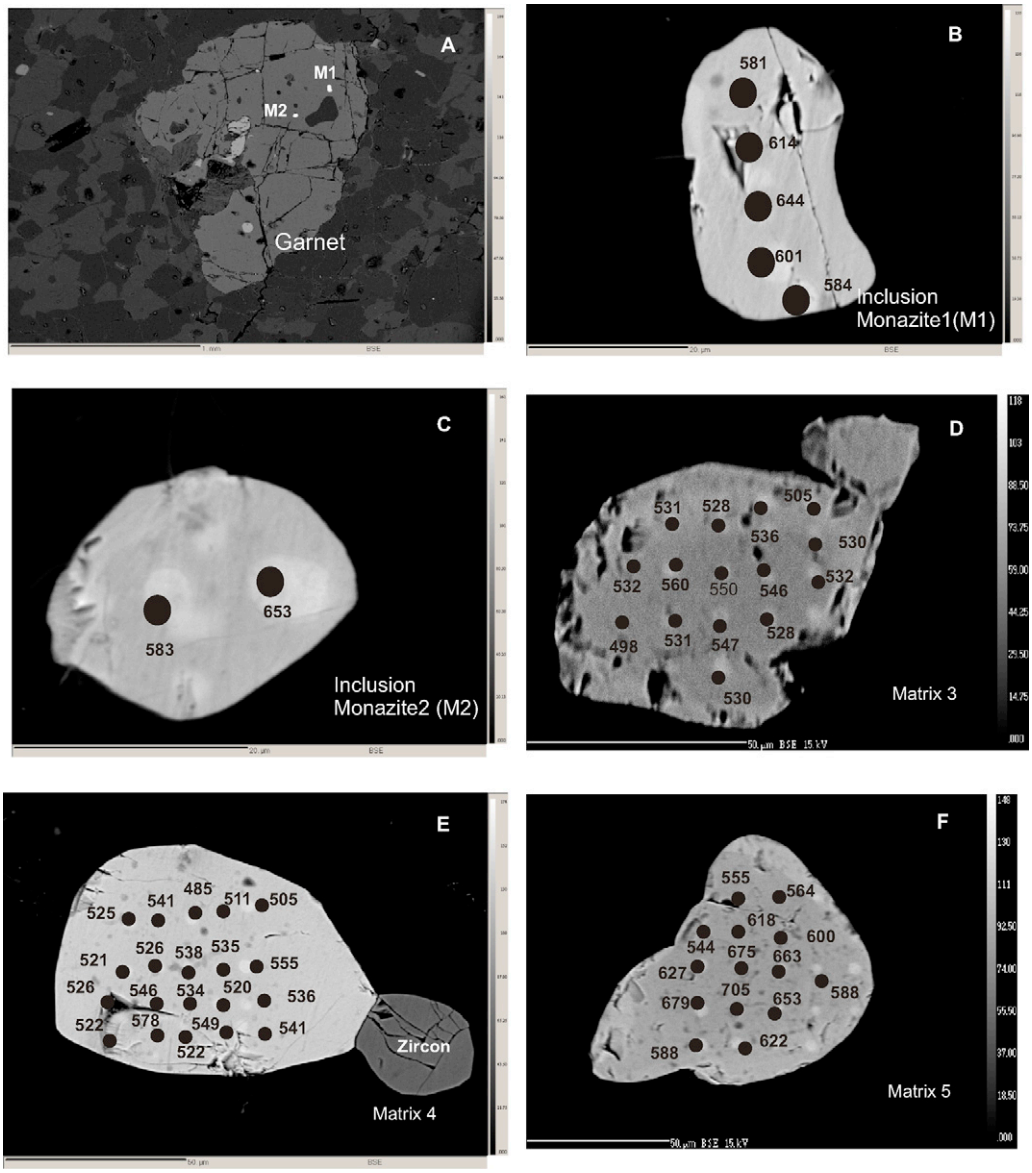

Fig. 8. (A) Subhedral garnet with monazite inclusions in high melt garnet sillimanite gneiss. Note retrogressed biotite partially rimming it and matrix composed of K feldspar, plagioclase and quartz. There are two monazite grains (M1 and M2) included within the garnet which appear as bright spots in this BSE image. (B and C) Monazite grains M1 and M2 with spot ages. Note subhedral nature of monazite. (D–F) Matrix grains 3, 4 and 5 with spot ages. Note subhedral nature of grains 3 and 4 and anhedral nature of grain 5. Spot ages in grain 5 are slightly older.

both the bulk compositions. Considering assemblages in different protolith compositions (metapelites, garnet–clinopyroxene gneiss and mafic granulite), multiple geothermobarometers and the pseudosection analyses the peak preserved metamorphic conditions for granulites in the Humboldt Mountains appears to be ~800 to 850 °C at 6–8 kbar pressure.

7. Monazite geochronology

A total of eight monazite grains were subjected to chemical dating using electron microprobe geochronology in two samples of garnet–sillimanite gneiss. Two of these grains occur in the matrix of CH-1 and their locations are shown in Fig. 7 which is a back scattered electron (BSE) image of the thin section compiled from over 80 individual overlapping scanning electron microscope generated images. Monazite A occurs parallel to the main foliation defined by quartz, K-feldspar, prismatic sillimanite and quartz. Plagioclase content (and thereby melt) in this sample is relatively rare. Grain C occurs juxtaposed to garnet overgrowth over an inner garnet which has profuse fibrolite and quartz inclusions. In the lower inset a BSE image of a part of sample CH-51 representing garnet sillimanite gneiss with high melt content shows monazite in the matrix amidst the quartz + plagioclase representing the melt composition. Out of the three inclusion monazites in high melt garnet sillimanite gneiss two grains are shown in Fig. 8A within garnet and their spot ages are given in Fig. 8B and C. The grains are subhedral. The three matrix grains in this rock with spot ages are shown in Fig. 8D–F. Two of these grains are subhedral while the third grain (Fig. 8F) is anhderal and it displays older ages. Two matrix monazite grains from the low melt garnet sillimanite gneiss with spot ages and their Y Lα maps are shown in Fig. 9. In the low melt garnet sillimanite gneiss, deeply embayed garnet and two-stage growth of garnet is present (Fig. 3F and BSE map of thin section). Resorption of garnet has been shown to release Y which is often accommodated in monazite (e.g. Gibson et al., 2004; Dahl et al., 2005) which is the likely cause of Y-enrichment in monazite.

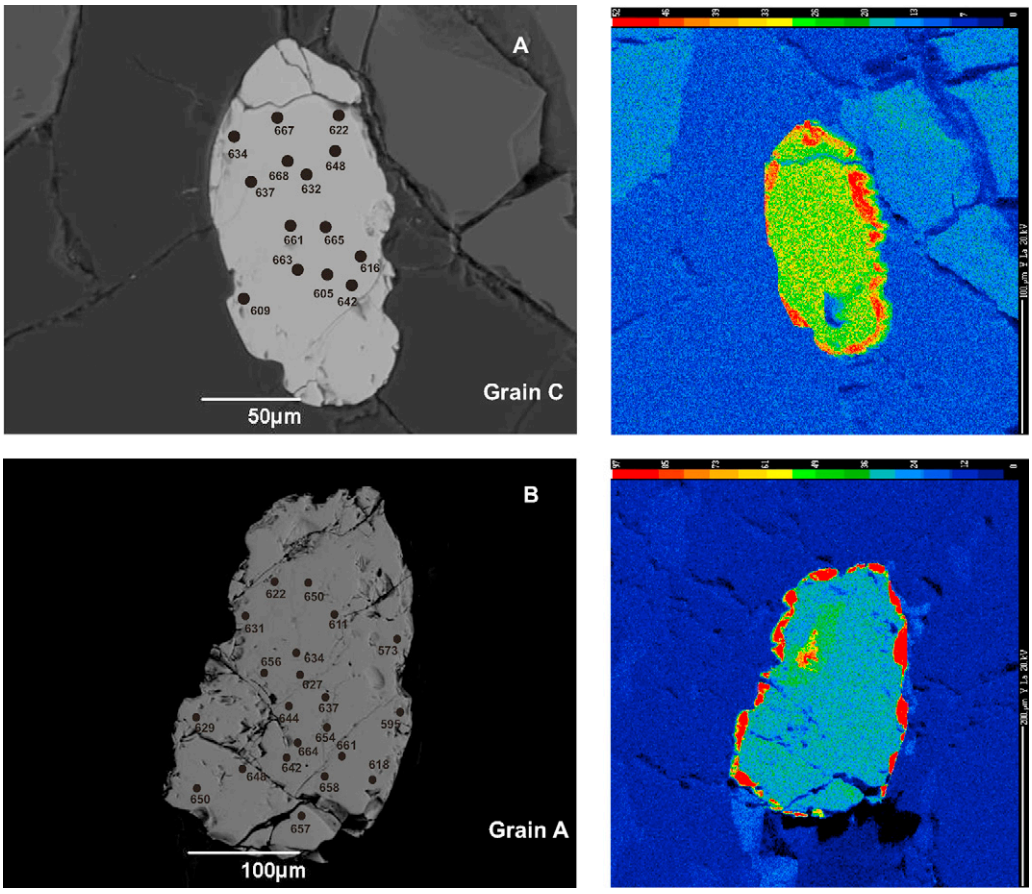

Fig. 9. (A and B) Spot ages and Y Lα X-ray maps of two matrix monazite grains in low melt garnet sillimanite gneiss. Note Y enriched margins of monazite corresponding to younger spot ages (573–595 Ma) possibly reflecting garnet resorption leading to Y-enrichment at the margins.

Chemical dating of monazite was carried out at the Electron Probe Microanalyser National Facility, Department of Geology and Geophysics, Indian Institute of Technology, Kharagpur and at EPMA Laboratory, Geological Survey of India, Faridabad. In both the electron microprobe is 4-spectrometer CAMECA SX 100 instrument. Calibrations were carried out at 20 kV and 20 nA, while analyses were obtained at the same high voltage but with a 200 nA current as it has been shown that calibrations at 20 nA as well at 200 nA yielded similar results (Pant et al., 2009). Pb Mα was measured on LPET and the peak counting time was 300 s with background measured on both sides. For uranium, U Mβ line was used in order to avoid interference with Th Mβ line with a peak counting time of 200 s. Thorium Mα peak was also counted for 200 s. Both these elements were measured on PET crystal. Rare Earth elements measured and the X-ray lines used included La (Lα), Ce (Lα), Nd (Lα), Pr (Lβ), Sm (Lα), Ho (Lβ), Dy (Lα) and Gd (Lβ). Positions for background measurements were arrived at using method of Reed and Buckley (1996). Counting time at the peak varied between 40 and 60 s for these elements. Y Lα line was used for yttrium and it was counted for 40 s on peak. Interference of Y Lλ on Pb Mα and Th Mζ on Pb Mα was corrected after measuring the interfering lines during calibration and thereafter applying the overlap correction.

Standards used for Pb, U and Th were PbS, UO_2 and ThO_2. Synthetic silica-aluminium glass containing 4% rare earth elements were used as standards for La, Ce, Nd, Pr, Sm, Ho, Dy and Gd. Phosphorus was calibrated with apatite. For Y, yttrium aluminium garnet (YAG) was used. Al and Fe were calibrated using corundum and hematite while for silica orthoclase was used. Further details of the analytical procedure are given in Pant et al. (2009). Complete analyses of monazite were obtained for chemical dating and the results with Si + P + S value at ~1.0 (normalization of cations at 4 O basis) were used for further processing. For individual spot ages, the formulation of Montel et al. (1996) was followed, whereas the age probability plots and unmixing of ages were obtained using the software Isoplot3 (v.3.71.09.06.19nx) (Ludwig, 2001, 2003). Uncertainties in individual analyses in the data table and in weighted mean ages are quoted at the 95% confidence level (2σ). The age estimations were simultaneously checked against two monazite grains of 2645 and 487 Ma ages, dated by Isothermal Dilution Thermal Ionisation Mass Spectrometry (Crowley et al., 2005; Chatterjee et al., 2007) and that of the Progress Granite from Antarctica (ref.). The ages obtained by chemical dating of these two grains are 2693 ± 96 and 506 ± 45 Ma. Representative monazite chemical compositions are given in Electronic Appendix (supplementary Tables 2A and 2B) and the salient compositional features are mentioned below.

Chemically all the analysed monazites are Ce-monazites. Since garnet–sillimanite gneiss preserves the melting reactions involving vapour-absent melting of biotite ((R3) and (R4)), it is possible to estimate the time of monazite formation using chemical compositions of these grains combined with their Th–U–Pb chemical dating. Since garnet sillimanite gneiss preserves evidence of rock experiencing temperatures in excess of hydrous melting curve and indication of biotite melting and considering the textural controls available for analysed monazite grains it is possible to relate monazite chemistry to the time of its formation. In the two samples of garnet–sillimanite gneiss, CH-51 exhibits evidence of extensive melting and crystallization while granitic melt proportion in CH-1 is significantly less. In the former two distinct monazite compositions are seen in the inclusion grains (ThO_2 as 3–6% and 8–9%; Supplementary table 2A) while the matrix grains are only low ThO_2

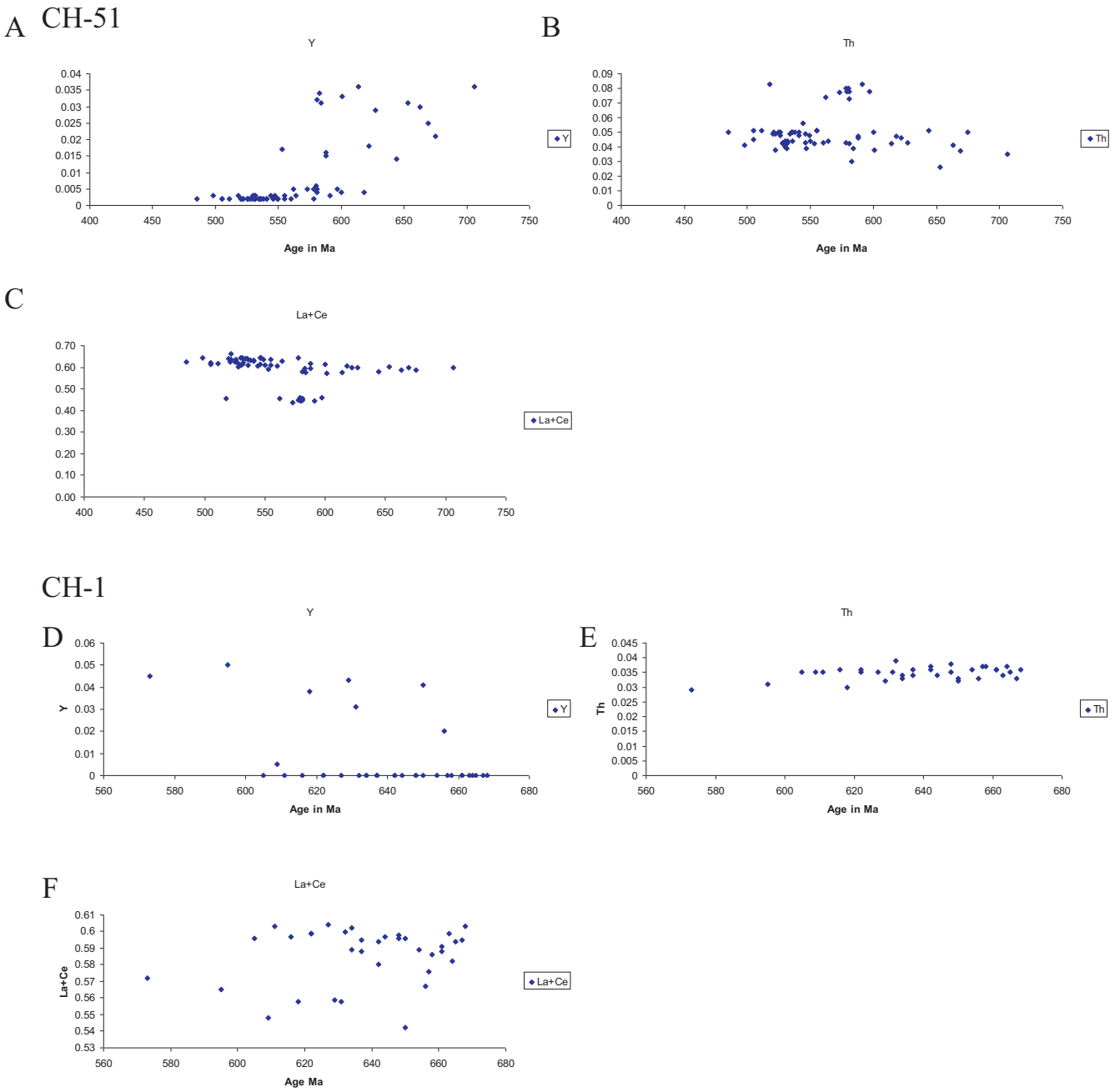

Fig. 10. Plot of age verus Y, Th and La + Ce (values on atoms per formula units (apfu) calculated on 4 oxygen basis) for monazites from high melt (CH51) and low melt (CH1) garnet sillimanite gneiss. Please see text for details.

(3–6%; Supplementary Table 2B). In CH-1 no monazite with high ThO_2 is analysed. Behaviour of yttrium, thorium and major light rare earth elements (La + Ce) is evaluated against age determined from chemical geochronology in plots of age versus cations (atoms per formula units, a.p.f.u. on 4 (O) basis; Fig. 10). The range of ages obtained varies between 670 and 500;Ma. There are some differences in the high melt (CH-51) and low melt (CH-1) samples. Yttrium in CH-51 shows variability in domains which are older than 580 Ma while younger age domains have a relatively uniform and very low Y content (Fig. 10A). Though Th and La + Ce in high melt sample show a relatively undisturbed trend, a decoupling at ~580 Ma is indicated by clustering of data points (Fig. 10B and C) and restricted variation of Th content in domains younger than 580 Ma. Restricted Y and Th compositions for younger age domains may imply fluid present growth possibly resultant from biotite dehydration melting. In CH-1 monazites Y and La + Ce are highly variable while Th is high and in a narrow range (Fig. 10D, E and F). The age data has been unmixed for three monazite grains included in garnet and dominant fraction (94%) indicates the age of 583 ± 10 Ma (Fig. 11) indicating the possible time of 2nd stage garnet growth isolation of included monazite from the matrix grains. The growth of monazite appears to have commenced ~670 to 650 Ma as within the texturally conformable monazite La + Ce and Th do not show abrupt changes. Unmixing of ages of the three matrix grains in the high melt sample shows an earlier population of 649 ± 24 Ma strongly (83%) overprinted by a later, thermal event at 537 ± 9 Ma. In the low-melt sample there is only one population of age for the two matrix monazite grains at 638 ± 10 Ma (Fig. 11) which is quite similar to the older age obtained in the high melt sample and since the monazite grains in the matrix of

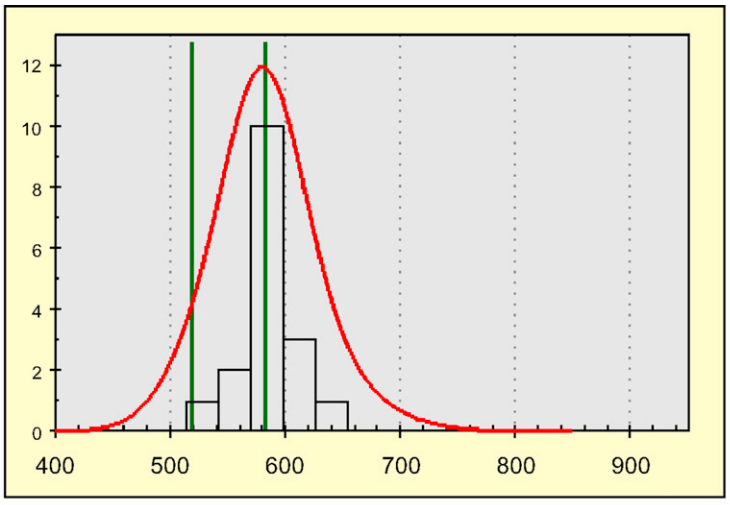

Age	±2σ	fraction	±2σ
519	32	0.06	0.13
583.2	9.5	0.94	---

relative misfit = 0.946

Monazite included in garnet

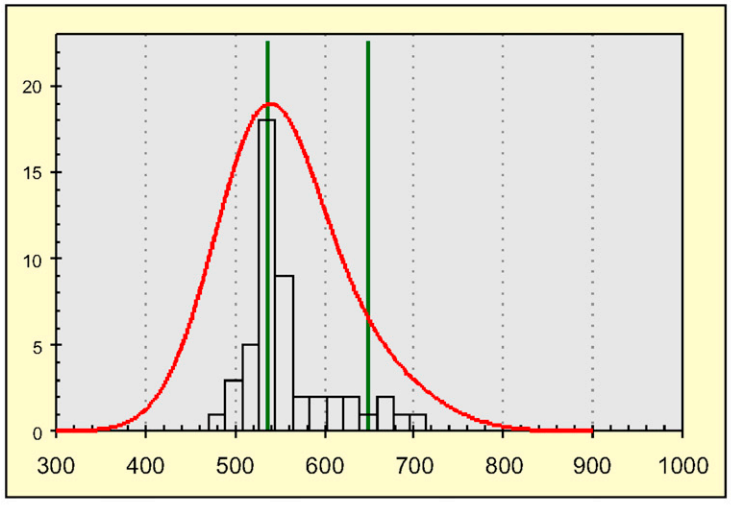

Age	±2σ	fraction	±2σ
536.8	9.2	0.83	0.26
649	24	0.17	---

relative misfit = 0.882

Monazite grains (3) from matrix

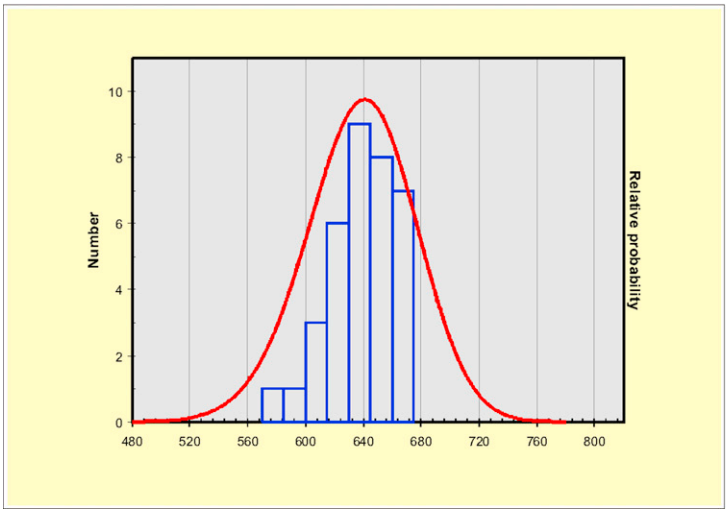

Mean = 638±10 [1.6%] 95% conf.
Wtd by data-pt errs only, 0 of 35 rej.
MSWD = 0.54, probability = 0.99

Fig. 11. (A) Age unmixed plot of three monazite grains included within garnet in CH51. (B) Age unmixed plot of three monazite grains from matrix in CH51. (C) Weighted average plot at 95% confidence level of the two matrix monazite in CH1.

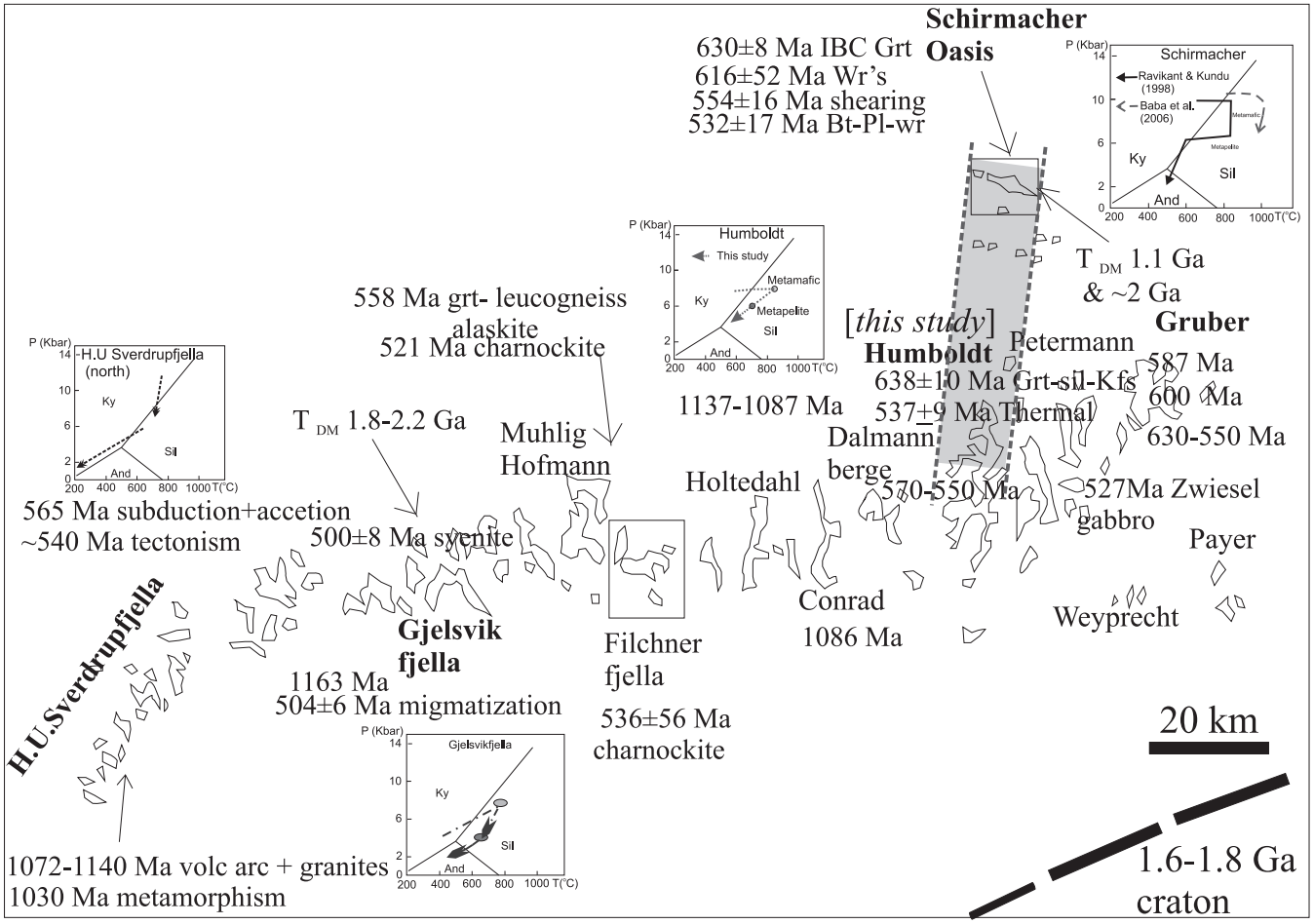

Fig. 12. A compilation of petrological and gechronological data from CDML (modified from Ravikant, 2008). Note the wide spread of Pan-African age anorogenic magmatic activity while the EAO (600–660) granulite grade metamorphism is restricted to the zone linking Schirmacher and the Humboldt mountains in CDML. The inferred extension of EAO marking suture of east and west Gondwana is shown by shaded area.

this sample are well constrained with the major peak metamorphic assemblage, this marks the age of the peak granulite facies metamorphism in these metapelites. Large scale anorogenic magmatism in form of granites and charnockites has been reported from the CDML (Joshi et al., 1991; Joshi and Pant, 1995) which has been dated between 500 and 550 Ma (Mikhalasky et al., 1997; Ravindra and Pandit, 2000) and this can be correlated with the younger thermal event in these monazites.

8. Discussion

The continent–continent collision marking the closure of the Mozambique Ocean occurred in between Zimbabwe–Kaapwal–Grunehogna and East Gondwana and both had ~1.1 Ga mobile belts rimming. Using the data-set of IGCP 288 (Wolmarans, 1999) and combining it with the continental fit for Gondwana proposed by Reeves and De Wit (2000), a composite Lurio-Vijayan block was envisaged which forms a peninsula of the Kalahari Block (Fig. 1 of Collins and Pisarevsky, 2005). A progressively higher grade of metamorphism in the Lurio-Vijayan peninsula to the south and evidence for 620–510 Ma magmatic, metamorphic and deformation events have been reported (Grantham et al., 1995; Jacobs et al., 2003; Ravikant et al., 2004; Macey et al., 2010) which led Jacobs et al. (1998) to suggest extension of EAO to CDML. However, proving this extension required establishing the equivalence of age of granulite grade metamorphism in CDML to that of the Lurio-Vijayan Block.

Monazite electron microprobe dating has been successfully used to date the metamorphism in several medium, high grade and ultra-high temperature terrains and has found widespread acceptance in recent times (Kelsey et al., 2007; Santosh et al., 2006, 2008; Bhandari et al., 2011; Jayananda et al., 2011; Saha et al., 2011). Using this technique we demonstrate the presence of granulites from several different bulk compositions in CDML. Mafic granulites are present within it. The metamorphic neocrystallization began in Neoproterozoic time (~640 to 650 Ma) and continued upto ~580 Ma extending for ~60 Ma and was marked by development of low to intermediate pressure granulite grade assemblages, partial melting and generation of in situ crystallization of granitic melt by biotite dehydration melting. The protracted metamorphism was overprinted by a strong thermal imprint at ~540 Ma and it is correlatable with large scale charnockite and A-type granite emplacements. Similar metamorphic history has been reported from Schirmacher oasis ~80 km to the north (Ravikant, 2005; Ravikant et al., 2007) indicating the Neoproterozoic granulite grade metamorphism to be of regional nature. Extensive pan-African thermal imprint in this terrain is evident manifested by anorthosite (~600 Ma), charnockite and anorogenic granite. The range of ages for charnockites and anorgenic granites is within 500–550 Ma (Mikhalasky et al., 1997) and it is possible that the AMCG magmatism in Dronning Maud Land may have taken place in more than one pulse. A compilation of metamorphic P–T–t paths and reported ages from Dronning Maud Land (Fig. 12) shows that the 500–600 Ma magmatic activity is widespread in the Dronning

Maud Land. However, granulite grade metamorphism of Neoproterozoic age (~640 Ma) is restricted to the Schirmacher oasis and the Humboldt Mountains in CDML. Inferring kyanite to fibrolite and subsequent development of prismatic sillimanite + perthite in garnet–sillimanite gneiss and two pyroxene + garnet granulite from hornblende in mafic granulite, a near isobaric heating is indicated during the prograde metamorphism in the Humboldt Mountains (Fig. 12). The absence of significant decompression textures and the computed P–T indicates the retrograde path to be of moderate slope in P–T space. Though there are some differences in P–T–t paths inferred from the Schirmacher oasis and the Humboldt Mountain granulites both indicate an initial isobaric heating (continental collision and crustal thickening) reaching upto the sillimanite stability field followed by unroofing, thus, defining clockwise P–T–t paths (Fig. 12). The younger magmatic activity, spread on both east and west of the narrow zone of ~640 Ma granulites, shows anorogenic characters (Joshi et al., 1991; Joshi and Pant, 1995) and appears to be unrelated to the granulites. The zone of ~640 Ma granulite grade metamorphism is inferred as the remnant of suture between east and west Gondwana, shown as a shaded region in Fig. 12, provides the petrologic and geochronologic evidence of inland extension of EAO in CDML. The reported Mesoproterozoic age of metamorphism inferred from zircon overgrowth in orthogneisses/sheeted metagranite (Jacobs et al., 1998) is not consistent with the texturally constrained monazite ages and may represent either a detrital imprint or an earlier reworked component.

Acknowledgements

Sonalika Joshi and Aloka Dey are thanked for assistance in electron microprobe analysis. Part of the analytical work was carried out at DST funded National Facility at the Department of Geology and Geophysics, IIT Kharagpur. Dr. B. Chattopadhyay facilitated EPMA analysis at Geological Survey of India, Faridabad. AK and MJD thank the Director General, Geological Survey of India for permitting the publication. Mayuri Pandey helped in calculations. The samples were collected during Indian Scientific Expeditions to Antarctica. Valuable critical comments by anonymous reviewers have greatly improved the contents of the paper.

Appendix A. Supplementary data

Supplementary data associated with this article can be found, in the online version, at http://dx.doi.org/10.1016/j.precamres.2012.06.013.

References

Baba, S., Owada, M., Grew, E.S., Shiraishi, K., 2006. Sapphirine granulite from Schirmacher Hills, Central Dronning Maud Land. In: Fütterer, D.E., Damaske, D., Kleinschmidt, G., Miller, H., Tessonsohn, F. (Eds.), Antarctic Contributions to Global Earth Science. Springer, Berlin, pp. 37–44.

Baba, S., Owada, M., Shiraishi, K., 2008. Contrasting metamorphic P–T path between Schirmacher Hills and Mühlig-Hofmannfjella, central Dronning Maud Land, East Antarctica. In: Satish-Kumar, M., Motoyoshi, Y., Osanai, Y., Hiroi, Y., Shiraishi, K. (Eds.), Geodynamic Evolution of East Antarctica: A Key to the East–West Gondwana Connection. Geological Society of London, Special Publication, 308, pp. 401–417.

Baba, S., Hokada, T., Kaiden, H., Dunkley, D.J., Owada, M., Shiraishi, K., 2010. SHRIMP zircon U–Pb dating of sapphirine-bearing granulite and biotite–hornblende gneiss in the Schirmacher Hills, East Antarctica: implications for Neoproterozoic ultrahigh-temperature metamorphism predating assembly of Gondwana. Journal of Geology 118, 621–639.

Bertrand, P., Mercier, J.-C.C., 1985. The mutual solubility of coexisting ortho- and clinopyroxene: toward an absolute geothermometer for the natural system? Earth and Planetary Science Letters 76, 109–122.

Bhandari, A., Pant, N.C., Bhowmik, S.K., Goswami, S., 2011. ~1.6 Ga ultrahigh-temperature granulitemetamorphism in the Central Indian Tectonic Zone: insights from metamorphic reaction history, geothermobarometry and monazite chemical ages. Geological Journal 46, 198–216.

Bhattacharya, A., Mohanty, L., Maji, A., Sen, S.K., Raith, M., 1992. Non-ideal mixing in the phlogopite–annite binary: constraints from experimental data on Mg–Fe partitioning and a reformulation of the biotite–garnet geothermometer. Contributions to Mineralogy and Petrology 111 (1), 87–93.

Binns, R.A., 1968. Hydrothermal investigations of the amphibolites granulite facies boundary. Geological Society of Australia Special Publication 2, 341–344.

Bisnath, A., Frimmel, H.E., Armstrong, R.A., Board, W.S., 2006. Tectono-thermal evolutionof the Maud Belt: new SHRIMP U–Pb zircon data from Gjelsvikfjella, Dronning Maud Land, Antarctica. Precambrian Research 150, 95–121.

Boger, S.D., 2011. Antartica – before and after Gondwana. Gondwana Research 19, 335–371.

Bohlen, S.R., Boettcher, A.L., Wall, V.J., Clemens, J.D., 1983. Stability of phlogopite-quartz and sanidine-quartz: a model for melting in the lower crust. Contributions to Mineralogy and Petrology 83, 270–277.

Bohlen, S.R., Liotta, J.J., 1986. A barometer for garnet amphibolites and garnet granulites. Journal of Petrology 27 (5), 1025–1034.

Chatterjee, N., Mazumdar, A.K., Bhattacharya, A., Saikia, R.R., 2007. Mesoproterozoicgranulites of the Shillong–Meghalaya Plateau: evidence of westward continuation of the Prydz Bay Pan-African suture into northeastern India. Precambrian Research 152, 1–26.

Collins, A.S., Pisarevsky, S.A., 2005. Amalgamating eastern Gondwana: the evolution of the Circum-Indian Orogens. Earth Science Reviews 71, 229–270.

Collins, A.S., Kinny, P.D., Razakamanana, T., 2012. Depositional age, provenance and metamorphic age of sedimentary rocks from southern Madagascar. Gondwana Research 21, 353–361.

Connolly, J.A.D., 1990. Multivariable phase diagrams: an algorithm based on generalized thermodynamics. American Journal of Science 290 (2012), 666–718.

Crowley, J.L., Myers, J.S., Sylvester, P.J., Cox, R.A., 2005. Detrital zircon from the Jack Hills and Mount Narryer, Western Australia: evidence for diverse >4.0 Ga source rocks. Journal of Geology 113, 239–263.

Dahl, P.S., 1980. Thermal—compositional dependence of Fe^{+2}–Mg distribution between co-existinggarnet and pyroxene: applications to geothermometry. American Mineralogist 66, 852–866.

Dahl, P.S., Terry, M.P., Jercinovic, M.J., Williams, M.L., Hamilton, M.A., Foland, K.A., Clement, S.M., Friberg, L.M., 2005. Electron probe (Ultrachron) microchonometry of metamorphic monazite: unravelling the timing of polyphase thermotectonism in the easternmost Wyoming Craton (Black Hills, South Dakota). American mineralogist 76, 148–160.

Eckert Jr., J.O., Newton, R.C., Kleppa, O.J., 1991. ΔH of reaction and recalibration of garnet pyroxene–plagioclase–quartz geobarometers in CMAS system by solution calorimetry of stoichiometric mineral mixes. American Mineralogist 76, 148–160.

Ellis, D.J., Green, D.H., 1979. An experimental study of the effect of Ca upon garnet-clino pyroxeneFe–Mg exchange equilibria. Contributions to Mineralogy and Petrology 71, 13–22.

Ferry, J.M., Spear, F.S., 1978. Experimental calibration of the partitioning of Fe and Mg between biotite and garnet. Contributions to Mineralogy and Petrology 66 (2), 113–117.

Fitzsimons, I.C.W., 2000a. Grenville-age basement provinces in East Antarctica: evidence for three separate collisional orogens. Geology 28, 879–882.

Fitzsimons, I.C.W., 2000b. A review of tectonic events in the East Antarctic Shield and their implications for Gondwana and earlier supercontinents. Journal of African Earth Sciences 31 (1), 3–23.

Fyfe, 1970. Some thoughts on granitic magma. In: Newal, G., Rast, N. (Eds.), Mechanism of Igneous Intrusion. Geological Journal 2, 201–216 (Special Issue).

Ganguly, J., 1979. Garnet and clinopyroxene solid solutions and geothermometry based on Fe–Mg distribution coefficient. Geochimica Cosmochimica Acta 43, 1021–1029.

Ganguly, J., Saxena, S.K., 1984. Mixing properties of alumino-silicate garnets: constraints from natural and experimental data and applications to geothermometry. American Mineralogist 69 (1–2), 88–97.

Gibson, D.H., Carr, S.D., Brown, R.L., Hamilton, M.A., 2004. Correlations between chemical and age domains in monazite and metamorphic reactions involving major politic phases: an integration of ID-TIMS and SHRIMP geochronology with Y–Th–U X-ray mapping. Chemical Geology 211, 237–260.

Goergen, E.T., Whitney, D.L., Zimmerman, M.E., Hiraga, T., 2008. Deformation-induced polymorphic transformation: experimental deformation of kyanite, andalusite, and sillimanite. Tectonophysics 454, 23–35.

Goldman, D.S., Albee, A.L., 1977. Correlation of Mg/Fe partitioning between garnet and biotite with partitioning between quartz and magnetite. American Journal of Science 277 (6), 750–767.

Golynsky, A., Jacobs, J., 2001. Grenville age versus Pan-African magnetic anomaly imprints in western Dronning Maud Land, East Antartica. Journal of Geology 109, 136–142.

Grantham, G.H., Jackson, C., Moyes, A.B., Groenewald, P.B., Harris, P.D., Ferrar, G., Krynauw, J.R., 1995. The tectonothermal evolution of the Kirwanveggen—H.U. Sverdrupfjella areas, Dronning Maud Land, Antarctica. Precambrian Research 75 (3–4), 209–229.

Grew, E.S., 1981. Surinamitg taaffeite and beryllian sapphirine from pegmatites in granulitefaciesrocks of Casey Bay, Enderby Land, Antarctica. American Mineralogist 66, 1022–1033.

Groenewald, P.B., Moyes, A.B., Grantham, G.H., Krynauw, J.R., 1995. East Antarctic crustal evolution: geological constraints and modelling in western Dronning Maud Land. Precambrian Research 75 (3-4), 231–250.

Helgeson, H.C., Delany, J.M., Nesbitt, H.W., Bird, D.K., 1978. Summary and critique of the thermodynamic properties of the rock forming minerals. American Journal of Science 278A, 1–299.

Harley, S.L., 1984a. The solubility of alumina in orthopyroxene coexisting with garnet in FeO–Al_2O_3–SiO_2 and GaO–MgO–FeO–Al_2O_3–SiO_2. Journal of Petrology 25, 665–696.

Harley, S.L., 1984b. An experimental study of the partitioning of Fe and Mg between garnetand orthopyroxene. Contributions to Mineralogy and Petrology 86, 359–373.

Hodges, K.V., Spear, F.S., 1982. Geothermometry, geobarometry and the Al_2SiO_5 triple point at Mt. Moosilauke, New Hamushire. American Mineralogist 67 (1–12), 1118–1134.

Hodges, K.V., Crowley, P.D., 1985. Error estimation and empirical geothermobarometry forpelitic systems. American Mineralogist 70 (7-8), 702–709.

Holdaway, M.J., Lee, S.M., 1977. Fe–Mg cordierite stability in high grade pelitic rocks based on experimental, theoretical and natural observations. Contributions to Mineralogy and Petrology 63 (2), 175–198.

Hoffman, P.F., 1991. Did the breakout of Laurentia turn Gondwanaland inside out? Science 252, 1409–1412.

Holland, T.J.B., Powell, R., 1998. An internally-consistent thermodynamic dataset for phases of petrological interest. Journal of Metamorphic Geology 16, 309–344.

Holland, T.J.B., Powell, R., 2003. Activity-composition relations for phases in petrological calculations: an asymmetric multi component formulation. Contributions to Mineralogy and Petrology 145, 492–501.

Indares, A., Martignole, J., 1985. Biotite–garnet geothermometry in the granulite facies: the influence of Ti and Al in biotite. American Mineralogist 70 (334), 272–278.

Jacobs, J., Fanning, C.M., Henjes-Kunst, F., Olesch, M., Paech, H.J., 1998. Continuation of the Mozambique Belt into East Antarctica: Grenville age metamorphism and polyphase Pan-African high grade events in Central Dronning Maud Land. Journal of Geology 106, 385–406.

Jacobs, J., Hansen, B.T., Henjes-Kunst, F., Thomas, R.J., Weber, K., Bauer, W., Armstrong, R.A., Cornell, D.H., 1999. New age constraints on the Proterozoic/lower Palaeozoic evolution of Heimefrontfjella, East Antarctica, and its bearing on Rodinia/Gondwana correlations. Terra Antartica 6, 377–389.

Jacobs, J., Klemd, R., Fanning, C.M., Bauer, W., Colombo, F., 2003. Extensional collapse of the late Neoproterozoic/early Palaeozoic East African/Antarctic Orogen in central Dronning Maud Land. Journal of the Geological Society of London Special Publication 206, 271–287.

James, P.R., Tingey, R.J., 1983. The Precambrian geological evolution of the East Antarctic metamorphic shield – a review. In: Oliver, R.L., James, P.R., Jago, J.B. (Eds.), Antarctic Earth Science. Canberra Australian Academy of Science, pp. 5–15.

Jayananda, M., Banerjee, M., Pant, N.C., Dasgupta, S., Kano, T., Mahesha, N., Mahabaleswar, B., 2011. 2.62 Ga high-temperature metamorphism in the central part of the Eastern Dharwar Craton: implications for late Archaean tectonothermal history. Geological Journal, http://dx.doi.org/10.1002/gj.1308.

Joshi, A., Pant, N.C., Parimoo, M.L., 1991. Granites of Petermann ranges, East Antarctica and implications on their genesis. Journal of Geological Society of India 38, 169–218.

Joshi, A., Pant, N.C., 1995. Petrology, geochemistry and evolution of the charnockite suite ofthe Petermann ranges, East Antarctica. In: Yoshida, M., Santosh, M. (Eds.), India and Antarctica during the Precambrian, vol. 34. Memoirs of Geological Society of India, pp. 241–258.

Kelsey, D.E., Hand, M., Clark, C., Wilson, C.J.L., 2007. On the application of in situ monazitechemical geochronology to constraining P–T–t histories in high-temperature (>850 °C) polymetamorphic granulites from Prydz Bay, east Antarctica. Journal of the Geological Society, London 164, 667–683.

Koziol, A.M., Newton, R.C., 1988. Redetermination of the anorthite breakdown reaction andimprovement of the plagioclase–garnet–Al_2SiO_5–quartz barometer. American Mineralogist 73 (34), 216–223.

Koziol, A.M., 1989. Recalibration of the garnetplagioclase–Al_2SiO_5–quartz (GASP) geobarometer and applications to natural parageneses. EOS Transactions, American Geophysical Union 70 (15), 493.

Kriegsman, L.M., Hensen, B.J., 1998. Back reaction between restite and melt: implications for geothermobarometry and pressure–temperature paths. Geology 26, 1111–1114.

Krogh, E.J., 1988. The garnet–clinopyroxene Fe–Mg geothermometer a reinterpretation of existing experimental data. Contributions to Mineralogy and Petrology 99, 44–48.

Larson, T.E., Zachary, S.D., 2001. Aluminium silicate polymorph transformations and the significance of fibrolite verses prismatic sillimanite. A Study from the 'Triple-Point Isobar', New Hampshire, GSA Annual Meeting, Paper No. 6-0.

Lavrent'eva, I.V., Perchuk, L.L., 1981. Phase correspondence in the system biotite–garnet: experimental data. Doklady Akademii Nauk SSSR 260, 731–734.

Leake, B., Wolley, A.R., Arps, C.E.S., Birch, W.D., Gilbert, M.C., Grice, J.D., Hawthorne, F.C., Kato, A., Kisch, H.J., Krivovichev, V.G., Linthout, K., Laird, J., Mandarino, J.A., Maresch, W.V., Nickel, E.H., Rock, N.M.S., Schumacher, J.C., Smith, D.C., Stephenson, N.C.N., Ungaretti, L., Whittaker, E.J.W., Youzhi, G., 1997. Nomenclature of amphiboles. Report of the subcommittee on amphiboles of the International Mineralogical Association: Commission on New Mineral Names. Mineralogical Magazine 61, 295–321.

Ludwig, K.R., 2001. Ludwig, Squid 1.02: a user manual. Berkeley Geochronological Center Special Publication 12, 19.

Ludwig, K.R., 2003. Isoplot 3.00: A Geochronological Toolkit for Microsoft Excel Berkeley. Berkeley Chronology Center Special Publication No. 4, California.

Macey, P.H., Thomas, R.J., Grantham, G.H., Ingram, B.A., Jacobs, J., Armstrong, R.A., Roberts, M.P., Bingen, B., Hollick, L., de Kock, G.S., Viola, G., Bauer, W., Gonzales, E., Bjerkgård, T., Henderson, I.H.C., Sandstad, J.S., Cronwright, M.S., Harley, S., Solli, A., Nordgulen, Ø., Motuza, G., Daud, E., Manhiça, V., 2010. Mesoproterozoic geology of the Nampula Block, northern Mozambique: tracing fragments of Mesoproterozoic crust in the heart of Gondwana. Precambrian Research 182 (1–2), 124–148.

McWilliams, M.O., 1981. Palaeomagnetism and Precambrian tectonic evolution of Gondwana. In: KrÖner, A. (Ed.), Precambrian Plate Tectonics. Elsevier, Amsterdam, pp. 649–687.

Meert, J.G., Van der Voo, R., Ayub, S., 1995. Palaeomagnetic investigation of the Neoproterozoic Gagwe lavas and Mbozi Complex, Tanzania and the assembly of Gondwana. Precambrian Research 74, 225–244.

Mikhalasky, E.V., Beliatsky, B.V., Savva, E.V., Wetzel, H.U., Fedorov, L.V., Weiser, T., Hahne, K., 1997. Reconnaissance geochronologic data on polymetamorphic and igneousrocks of the Humboldt Mountains, East Antarctica. In: Proc. 7th International Symposium on Antarctic Earth Sciences, pp. 45–53.

Mikhalasky, E.V., Sheraton, J.W., Hahne, K., 2006. Charnockite composition in relation to the tectonic evolution of East Antarctica. Gondwana Research 9 (4), 379–397.

Montel, J.M., Foret, S., Veschambre, M., Nicollet, C., Provost, A., 1996. Electron microprobe dating of monazite. Chemical Geology 131, 37–53.

Mori, T., Green, D.H., 1978. Laboratory duplication of phase equilibria observed in natural garnetherzolite. Journal of Geology 86, 83–97.

Mysen, B.O., Heier, K.S., 1972. Petrogenesis of eclogites in high grade metamorphic gneisses, exemplified by the Hareidland eclogite, Western Norway. Contributions to Mineralogy and Petrology 36, 73–94.

Nehru, C.E., Wyllie, P.J., 1974. Electron microprobe measurements of pyroxene coexisting with H_2O-undersaturated liquid in the join $CaMgSi_2O_6$–$MgSi_2O_6$–H_2O at 30 kbar, with applications to geothermometry. Contributions to Mineralogy and Petrology 48, 221–228.

Newton, R.C., Haselton, H.T., 1981. Thermodynamics of the garnet–plagioclase–Al_2SiO_5, quartz geobarometer. In: Newton, R.C., Navrotsky, A., Wood, B.J. (Eds.), Thermodynamics of Minerals and Melts, Advances in Physical Geochemistry, vol. 1. Springer-Verlag, New York, pp. 131–147.

Newton, R.C., Perkins, D., 1982. Thermodynamic calibration of geobarometers based on the assemblages garnet–plagioclase–orthopyroxene (clinopyroxene)–quartz. American Mineralogist 67, 203–222.

Pant, N.C., Verma, P.K., 1994. Grain growth parameters and mineral zoning: a comparative study from Humboldt Mountains, East Antarctica. Journal of Geological Society of India 44, 627–635.

Pant, N.C., Kundu, A., Joshi, S., Dey, A., Bhandari, A., Joshi, A., 2009. Chemical dating of monazite: testing of an analytical protocol against independently dated standards. Indian Journal of Geosciences 63, 311–318.

Pattison, D.R.M., Newton, R.C., 1989. Reversed experimental calibration of the garnet–clinopyroxene Fe–Mg exchange thermometer. Contributions to Mineralogy and Petrology 101, 87–103.

Paulsson, O., Austrheim, H., 2003. A geochronological and geochemical study of rocks from the Gjelsvikfjella, Dronning Maud Land, Antarctica—implications for Mesoproterozoic correlations and assembly of Gondwana. Precambrian Research 125, 113–138.

Perchuk, L.L., Lavrent'eva, I.V., 1983. Experimental investigation of exchange equilibria in the system cordierite–garnet–biotite. In: Saxena, S.K. (Ed.), Kinetics and Equilibrium in Mineral Reaction. Springer-Verlag, Berlin, pp. 199–239.

Perchuk, L.L., Aranovich, L.Y., Podlesskii, K.K., Lavrent'eva, I.V., Gerasimov, V.Y., Fed'Kin., V.V., Kitsul, V.I., Karasakov, L.P., Berdnikov, N.V., 1985. Precambrian granulites of the Aldan shield, eastern Siberia, USSR. Journal of Metamorphic Geology 3 (3), 265–310.

Perkins III, D., Chipera, S.J., 1985. Garnet–orthopyroxene–plagioclase–quartz geobarometry: refinements and application to the English River sub province and the Minnesota River Vallley. Contributions to Mineralogy and Petrology 89, 69–80.

Perkins, D., Newton, R.C., 1981. Charnockite geobarometers based on coexisting garnet pyroxene–plagioclase–quartz. Nature 292, 144–146.

Piper, J.D.A., 1976. Palaeomagnetic evidence for a Proterozoic supercontinent. Philosophical Transactions of the Royal Society of London, Series A 280, 469–490.

Powell, R., 1985. Regression diagnostics and robust regression in geothermometer/geobarometer calibration: the Fe–Mg exchange thermometer revisited. Journal of Metamorphic Geology 3, 231–243.

Powell, R., Holland, T.J.B., 1988. An internally consistent dataset with uncertainties and correlations; 3, applications to geobarometry, worked examples and a computer program. Journal of Metamorphic Geology 6, 173–204.

Raheim, A., Green, D.H., 1974. Experimental determination of the temperature and pressure dependence of the Fe–Mg partitioning coefficient for coexisting garnet and clinopyroxene. Contributions to Mineralogy and Petrology 48, 179–203.

Ravich, M.G., Soloviev, D.S., 1966. Geology and Petrology of the Mountain of the Central Queen Maud Land, Eastern Antarctica. Trans. Sci. Res. Inst. Arctic Geol., Leningrad, p. 141.

Ravich, M.G., Kamenev, E.N., 1975. Crystalline Basement of the Antarctic Platform. John-Wiley, NY, p. 582.

Ravikant, V., Kundu, A., 1988. Reaction textures of retrograde pressure–temperature–deformation paths from granulites of Schirmacher Hills, East Antarctica. Journal of the Geological Society of India 51 (3), 305–314.

Ravikant, V., Bhaskar Rao, Y.J., Gopalan, K., 2004. Schirmacher Oasis as an extension of the East African Orogen into Antarctica: new Sm–Nd isochron age constraints. Journal of Geology 112, 607–616.

Ravikant, V., 2005. Metamorphism of mafic and ultramafic enclaves within granulites, Schirmacher Oasis, East Antarctica. Journal of Geological Society India 65 (3), 279–290.

Ravikant, V., Laux, J.H., Pimentel, M.M., 2007. Sm–Nd and U–Pb isotopic constraints for crustal evolution during Late Neoproterozic from rocks of the Schirmacher Oasis, East Antarctica: geodynamic development coeval with the East African Orogeny, in Antarctica: a Keystone in a changing World-Online. In: Cooper, A.K., Raymond, C.R., et, al. (Eds.), Proceedings of the 10th ISAES, USGS Open-File Report 2007-1047, Short Research Paper 007., http://dx.doi.org/10.3133/of2007-1047.srp007, 5 p.

Ravikant, V., 2008. Late Neoproterozoic orogenesis in the Central Dronning Maud Land, East Antarctica: a review of tectonothermal events affecting rocks of the Schirmacher oasis. Geological Survey of India, Special Publication 91, 156–170.

Ravindra, R., Pandit, M.K., 2000. Geochemistry and geochronology of A-type granite from northern Humboldt Mountains, East Antarctica: vestige of Pan-African event. Journal of Geological Society of India 56, 253–262.

Reed, S.J.B., Buckley, A., 1996. Virtual WDS. Mikrochimica Acta (Supplement) 13, 479–483.

Reeves, C., De Wit, M.J., 2000. Making ends meet in Gondwana: retracing the transforms of the Indian Ocean and reconnecting continental shear zones. Terra Nova 12, 272–280.

Saha, L., Pant, N.C., Pati, J.K., Upadhyay, D., Berndt, J., Bhattacharya, A., Satynarayanan, M., 2011. Neoarchean high-pressure margarite–phengitic muscovite–chlorite corona mantled corundum in quartz-free high-Mg, Al phlogopite–chlorite schists from the Bundelkhand craton, north central India. Contributions to Mineralogy and Petrology 161 (4), 511–530.

Santosh, M., Sajeev, K., Li, J.H., 2006. Extreme crustal metamorphism during Columbia supercontinent assembly: evidence from North China Craton. Gondwana Research 10, 256–266.

Santosh, M., Tsunogae, T., Ohyama, H., Sato, K., Li, J.H., Liu, S.J., 2008. Carbonic metamorphism at ultrahigh-temperature: evidence from North China Craton. Earth and Planetary Science Letters 266, 149–165.

Sengupta, P., Dasgupta, S., Bhattacharya, P.K., Hariya, Y., 1989. Mixing behavior in quaternary garnet solid solution and an extended Ellis and Green garnet–clinopyroxene geothermometer. Contributions to Mineralogy and Petrology 103 (2), 223–227.

Spear, F.S., 1981. An experimental stability of hornblende stability and compositional variability in amphibolites. American Journal of Science 281, 697–734.

Stern, R.J., 1994. Arc assembly and continental collision in the Neoproterozoic East African Orogen: implications for the consolidation of Gondwana. Reviews in Earth and Planetary Sciences 22, 319–351.

Tajcmanova, L., Connolly, J.A.D., Cesare, B., 2009. A thermodynamic model for titanium and ferric iron solution in biotite. Journal of metamorphic Geology 27, 153–165.

Thompson, A.B., 1976. Mineral reactions in pelitic rocks: II. Calculation of some P–T–X (Fe–Mg) phase relations. American Journal of Science 276 (4), 425–454.

Thompson, A.B., 1982. Dehydration melting of politic rocks and the generation of H_2O-undersaturated granitic liquids. American Journal of Science 282, 1567–1595.

Williams, M.L., Grambling, J.A., 1990. Manganese, ferric iron and the equilibrium between garnet and biotite. American Mineralogist 75 (7-8), 886–908.

Wood, B.J., Bano, S., 1973. Garnet–orthopyroxene and orthopyroxene–clinopyroxene relationships in simple and complex systems. Contributions to Mineralogy and Petrology 42 (2), 109–124.

Wolmarans, L.G., 1999. Digital Data Set Resulting from IGCP Project 288 (Gondwanaland Sutures and Fold belts) Used in the Production of the Geodynamic Map of Gondwana Supercontinent Assembly. Council for Geosciences, South Africa.

Yoshida, M., Kizaki, K., 1983. Tectonic situation of Lützow-Holm Bay in East Antarctica and its significance in Gondwanaland. In: Oliver, R.L., James, P.R., Jago, J.B. (Eds.), Antarctic Earth Science. Australian Academy of Sciences Canberra, pp. 36–39.